An Evaluation of Contact Solution Algorithms

by

Seonghwa Park

Submitted to the Department of Civil and Environmental Engineering
in partial fulfillment of the requirements for the degree of

Master of Science in Civil and Environmental Engineering

at the

MASSACHUSETTS INSTITUTE OF TECHNOLOGY

February 2003

Author .....
Department of Civil and Environmental Engineering
January 17, 2003

Certified by .....
Klaus-Jürgen Bathe
Professor of Mechanical Engineering
Thesis Supervisor

Certified by .....
Jerome J. Connor
Professor of Civil and Environmental Engineering
Thesis Reader

Accepted by .....
Oral Buyukozturk
Chairman, Department Committee on Graduate Students

An Evaluation of Contact Solution Algorithms

by

Seonghwa Park

Submitted to the Department of Civil and Environmental Engineering
on January 17, 2003, in partial fulfillment of the
requirements for the degree of
Master of Science in Civil and Environmental Engineering

Abstract

In practical engineering analysis, considering contact effects is difficult due to the extreme complexity involved in contact phenomena, and therefore much effort has been expended to develop effective contact solution algorithms. However, efforts for an evaluation of the available algorithms have been relatively small. With this in mind, the segment method and the constraint function method are discussed in this thesis as contact solution algorithms. The algorithms are evaluated using the following three examples: (1) rectangular rubber block, (2) cylindrical rubber block and (3) rubber sheet in a converging channel. Moderate and large displacement conditions and frictional effects are considered. It is concluded that while good solutions have been obtained, clearly improvements in the algorithms are still desirable.

Thesis Supervisor: Klaus-Jürgen Bathe
Title: Professor of Mechanical Engineering

Thesis Reader: Jerome J. Connor
Title: Professor of Civil and Environmental Engineering

Acknowledgments

I would like to express my deep gratitude to my thesis supervisor, Professor Klaus-Jürgen Bathe, for his guidance and encouragement throughout my research work at M.I.T. His great ehthusiasm as a teacher is inspiring, and his wise suggestions regarding my thesis work were always very helpful.

I am also very grateful to my thesis reader, Professor Jerome J. Connor, for his valuable remarks concerning my work and his encouragement during my studies at M.I.T.

I would also like to thank my colleagues in the Finite Element Research group, Phill-Seung Lee, Jung-Wuk Hong, Muhammad Baig, Bahareh Banijamali and Jacques Olivier for their help and friendly support.

I am thankful to Nagi El-Abbasi in ADINA R&D, Inc for his assitance regarding my research.

I also wish to thank my best friend, Gwang-Sik Yoon for his constant encouragement and sincere friendship.

Finally, my utomost gratitude is due to my wife, Myunghee, my mother and all my family, whose love and understanding gave me the strength to complete this work.

Contents

List of Figures

Chapter 1

Introduction

Boundary value problems involving contact are of great importance in industrial applications in mechanical and civil engineering. It is also not surprising that contact interactions exist in virtually all structural and mechanical systems. The range of applications includes metal forming processes, drilling problems, bearings and crash analysis of cars or car tires. For example, metal forming processes could be analyzed to improve designs of the die assembly, or to obtain the structural strength of the final metal products. Other applications are related to biomechanics where human joints, implants or teeth are of consideration. Due to this variety, contact problems are today often combined either with large elastic or inelastic deformations including time dependent responses.

In engineering, contact interactions may be intentional such that a bridge structure can sustain loads or that a forging press can perform an assigned task. However, as in crash analysis of cars, there are situations where contact interactions are not intended. Because it is obvious that contact interactions may influence significantly the behavior of the structure or the mechanical system, it is important to have insight into the process of the interactions for increasing efficiency in intentional contact interactions and decreasing adverse effects in non-intentional contact interactions.

However, in practical engineering analysis, considering contact effects is difficult

because of the extreme complexity involved in contact phenomena as follows:

- Contact problems are inherently non-linear because contact conditions must be solved for together with the displacements of the system.

- Unlike other engineering problems, contact problems have unknown boundary conditions and typically these conditions evolve during the solution response.

- In contact analysis, the actual contacting surfaces and the stresses and displacements are all unknown prior to the solution of the problem.

- Due to the above facts, mathematical models of contact problems involve inequality constraints and nonlinear equations.

- Additionally, the interfacial behavior in the tangential direction (frictional response) is even more complicated and varies with the smoothness, chemical properties and temperature of the contacting surfaces.

To develop effective contact solution algorithms based on the common laws of Coulomb and Hertz, much literature on contact and friction problems has been published. Among recent numerical studies, there have been the works of Papadopoulos and Solberg [6], Zavarise and Wriggers [7], Wriggers and Krostulovic-Opera [9], Liu et al. [8] and El-Abassi and Bathe [4] and earlier works are published by Bathe and Chaudhary [2], Eterovic and Bathe [3], Kikuchi [10], Kikuchi and Song [11], Oden [12], Wriggers et al. [13], Glowinski et al. [14].

Considering the classes of solution methods, the most used methods are based upon Lagrange multiplier methods, penalty methods, and augmented Lagrangian methods.

In Lagrange multiplier methods, the contact pressure (Lagrange parameter) is treated as an independent variable. Among the above works, Papadopoulos and

Solberg [6], Bathe and Chaudhary [2], Eterovic and Bathe [3] and other authors have used Lagrange multiplier methods for contact problems.

In penalty methods, the contact condition is enforced in an approximate manner by a penalty function procedure. Kikuchi [10], Kikuchi and Song [11], Oden [12] have used these methods.

Augmented Lagrangian methods have been proposed as a procedure to partially overcome the drawback of Lagrange multiplier methods and penalty methods. Wriggers et al. [13], Glowinski et al. [14] have applied these methods to contact problems.

As described above, many contact algorithms have been suggested and developed but efforts for an evaluation of the algorithms have been relatively small. Hence, in this thesis, we will focus on and review the contact solution algorithms suggested by Bathe and Chaudhary [2], Eterovic and Bathe [3] among the algorithms and evaluate these algorithms through three examples.

The thesis outline is as follows. In Chapter 2 we review the continuum formulation of contact problems as the basis for finite element solutions, where equilibrium equations and contact conditions are included. In Chapter 3 we first describe basic solution approaches and then summarize and compare two contact solution algorithms, the segment method [2] and the constraint function method [3], which are implemented in the ADINA program. In Chapter 4, we present numerical solutions to evaluate the performance of finite element discretizations in three example problems. Finally, in Chapter 5, we close the presentation by giving the concluding remarks.

Chapter 2

Continuum Formulation

In this chapter, we briefly review the general continuum equilibrium equations including the contact conditions for finite element solutions [1]. We use the notations presented in [1].

2.1 Equilibrium Equations

We first consider a general solid body. Let us denote by S_u that part of S which contains the prescribed displacements applied on S, and by S_f that part of S to which surface tractions are applied. The body is also subjected to body forces in V. The solution to the problem must satisfy the following differential equations:

$$\tau_{ij,j} + f_i^B = 0 \qquad \text{in } V \tag{2.1}$$

$$\tau_{ij}\, n_j = f_i^{S_f} \qquad \text{on } S_f \tag{2.2}$$

$$u_i = u_i^{S_u} \qquad \text{on } S_u \tag{2.3}$$

where τ_{ij} are the components of the Cauchy stress tensor, a comma denotes differentiation, f_i^B are the externally applied body forces, n_j are the components of the unit normal vector to the surface S of the body, u_i denotes the ith displacement component, $S = S_u \cup S_f$ and $S_u \cap S_f = 0$.

The above equations can be recast into the following principle of virtual work equation

$$\int_V \tau_{ij}\ \bar{u}_{i,j}\ dV \ = \ \int_V f_i^B\ \bar{u}_i\ dV \ + \ \int_{S_f} f_i^{S_f}\ \bar{u}_i\ dS_f \tag{2.4}$$

where the overbar denotes virtual quantities, $f_i^{S_f}$ are the externally applied surface tractions.

If we use (2.4) for N bodies that are in contact, the principle of virtual work governing the conditions of the N bodies in the deformed configuration at time t is :

$$\begin{aligned}\sum_{L=1}^{N}\left\{\int_{{}^tV} {}^t\tau_{ij}\ \delta_t e_{ij}\ d^tV\right\} \ &= \ \sum_{L=1}^{N}\left\{\int_{{}^tV} \delta u_i\ {}^t f_i^B\ d^tV \ + \ \int_{{}^tS_f} \delta u_i^s\ {}^t f_i^{S_f}\ d^tS\right\} \\ &+ \ \sum_{L=1}^{N}\int_{{}^tS_c} \delta u_i^c\ {}^t f_i^c\ d^tS\end{aligned} \tag{2.5}$$

where $\delta_t e_{ij}$ are the virtual strain components corresponding to the virtual imposed displacements δu_i, ${}^t f_i^B$ are the components of the externally applied forces per unit volume, ${}^t f_i^{S_f}$ are the components of the known externally applied surface tractions, and ${}^t f_i^c$ are the components of the unknown contact tractions. We note that for each body, the known surface tractions act on the surface area ${}^tS_f$, the unknown contact tractions act on the unknown surface area ${}^tS_c$ which is to be calculated and the last summation sign gives the contribution of the contact forces.

2.2 Contact Conditions

Figure 2-1 shows conceptually the bodies I and J which are in contact and how contact tractions interact between two bodies, where we denote by ${}^t f^{IJ}$ the vector of contact surface tractions on body I due to contact with body J. By Newton's law of action and reaction, ${}^t f^{IJ} = -{}^t f^{JI}$. Hence, the last term of equation (2.5) corresponding to the surfaces S^{IJ} and S^{JI} in figure 2-1 can be represented as

$$\int_{S^{IJ}} \delta u_i^I\ {}^t f_i^{IJ}\ dS^{IJ} \ + \ \int_{S^{JI}} \delta u_i^J\ {}^t f_i^{JI}\ dS^{JI} \ = \ \int_{S^{IJ}} \delta u_i^{IJ}\ {}^t f_i^{IJ}\ dS^{IJ} \tag{2.6}$$

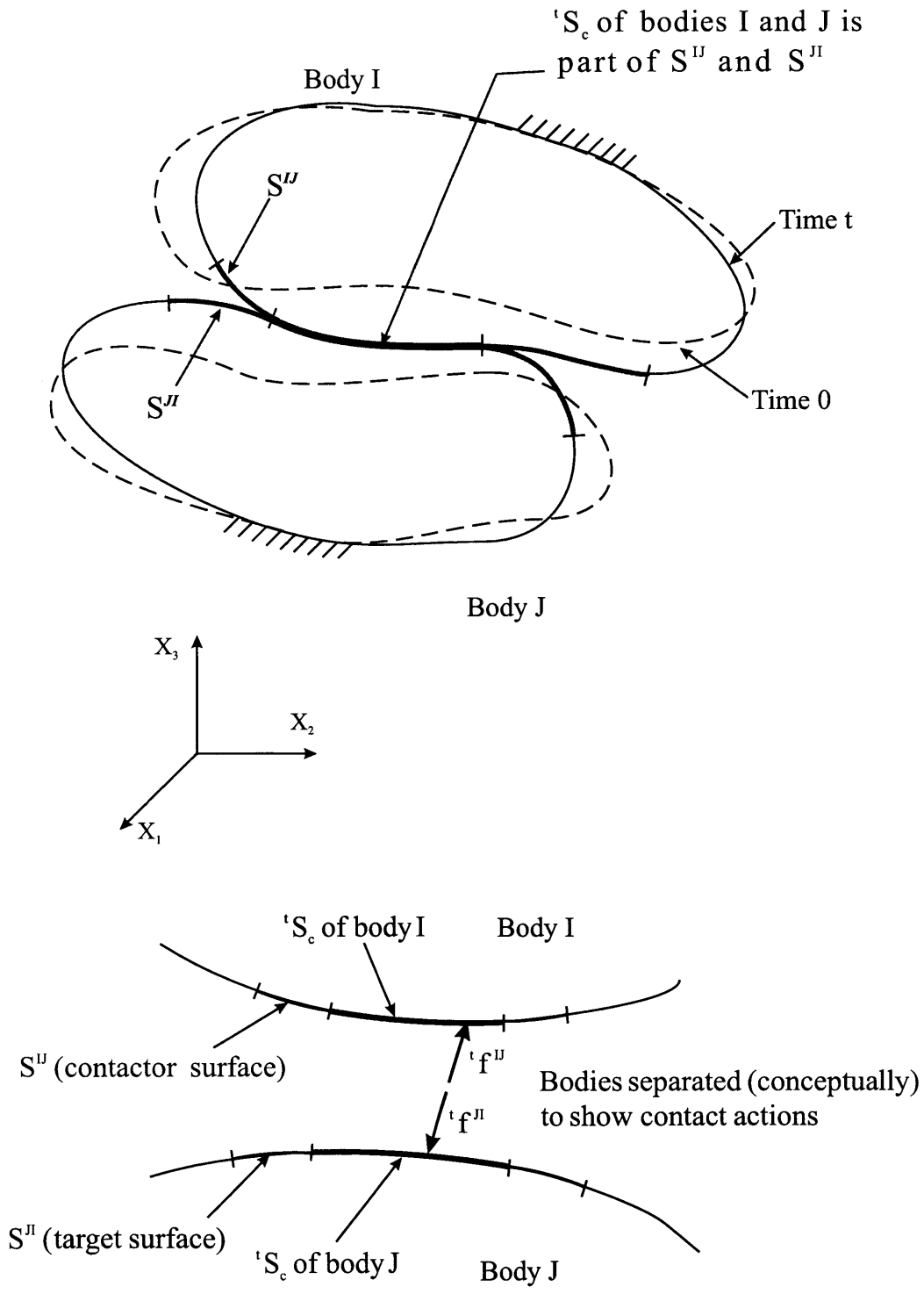

Figure 2-1: Bodies in contact at time t [1]

where we denote δu_i^I and δu_i^J as the virtual displacements on the contact surfaces of bodies I and J, respectively, and they satisfy the following equation

$$\delta u_i^{IJ} = \delta u_i^I - \delta u_i^J \tag{2.7}$$

Consider two contact surfaces like S^{IJ} and S^{JI} that are initially in contact or that are expected to come into contact during the response solution. We call each pair of the surfaces a "contact surface pair". Hence, the actual area(${}^tS^c$) of contact at time t for body I and J may be different from S^{IJ} and S^{JI} but in each case this area is part of S^{IJ} and S^{JI} (see Figure 2-1). One of the contact surfaces in the pair is designated to be the contactor surface(S^{IJ}) and the other contact surface is designated to be the target surface(S^{JI}).

Now we evaluate the right-hand side of equation (2.6). Figure 2-2 illustrates the definitions needed for this task. As shown in the figure, we denote by $\mathbf{n}$ the unit outward normal to S^{JI} and by $\mathbf{s}$ a vector such that $\mathbf{n}$, $\mathbf{s}$ form an orthonormal basis. We decompose the unknown contact traction ${}^t\mathbf{f}^{IJ}$ acting on S^{IJ} into normal and tangential components relative to S^{JI},

$${}^t\mathbf{f}^{IJ} = \lambda\mathbf{n} + t\mathbf{s} \tag{2.8}$$

where for the sake of clarity, we do not carry the superscripts I and J over the new variables to be defined for the contact pair, λ and t are the normal and tangential traction components satisfying the following relations:

$$\lambda = ({}^t\mathbf{f}^{IJ})^T\mathbf{n}; \qquad t = ({}^t\mathbf{f}^{IJ})^T\mathbf{s} \tag{2.9}$$

Next we analyze the contact conditions. First, no interpenetration should occur throughout the motion. Second, the normal contact tractions can only be compressive with the sign convention for λ positive for compression on the contact surfaces. We

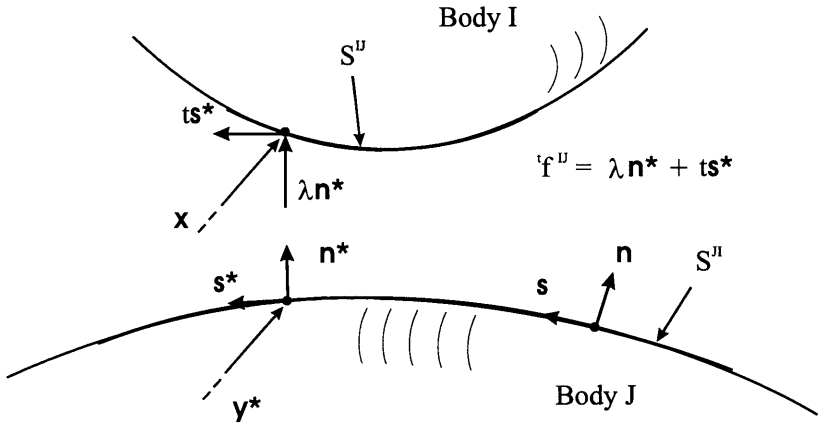

Figure 2-2: Definitions used in contact analysis [1]

consider a point $\mathbf{x}$ on S^{IJ} and let $\mathbf{y}^*(\mathbf{x}, t)$ be the point on S^{JI} satisfying

$$\|\mathbf{x} - \mathbf{y}^*(\mathbf{x}, t)\|_2 \;=\; \min_{y \in S^{JI}} \{\|\mathbf{x} - \mathbf{y}\|_2\} \tag{2.10}$$

We can obtain the (signed) distance from $\mathbf{x}$ to S^{JI} as follows, which is called the gap function for the contact surface pair. This function is one of main obstacles for an exact evaluation of contact problems [4]: In finite element solutions, this function is piecewise continuous along the contact surfaces but for a mesh of non-matching elements, changes in the slope occur at the nodes of either contact surface. Hence, this fact makes an exact evaluation for any integration scheme difficult. The gap function is

$$g(\mathbf{x}, t) \;=\; (\mathbf{x} - \mathbf{y}^*)^T \mathbf{n}^* \tag{2.11}$$

where the function g must be greater or equal to zero to satisfy the absence of interpenetration on the contact surfaces and $\mathbf{n}^*$ is the unit normal vector on $\mathbf{y}^*(\mathbf{x}, t)$.

Using these definitions, we can obtain the normal contact conditions which are given by

$$g \geq 0; \qquad \lambda \geq 0; \qquad g\lambda = 0 \tag{2.12}$$

The physical condition is that, if there is a gap between the two contact surfaces,

there can be no contact tractions. On the other hand, if the gap is zero, contact tractions will be initiated or are on the contact surfaces.

We shall assume that Coulomb's law of friction holds pointwise on the contact surface (although more representative friction laws are clearly desirable) and by this assumption, frictional effects are simplified. For tangential conditions, the nondimensional variable τ is defined as follows

$$\tau = \frac{t}{\mu\lambda} \tag{2.13}$$

where μ is the coefficient of friction between surfaces S^{IJ} and S^{JI}, $\mu\lambda$ is the frictional resistance, and the magnitude of the relative tangential velocity is given by

$$\dot{u}(\mathbf{x},t) = (\dot{\mathbf{u}}^J|_{y^*(\mathbf{x},t)} - \dot{\mathbf{u}}^I|_{(\mathbf{x},t)}) \cdot \mathbf{s}^* \tag{2.14}$$

where $\dot{\mathbf{u}}^I|_{(\mathbf{x},t)}$ is the velocity of point $\mathbf{x}$ at time t and $\dot{\mathbf{u}}^J|_{y^*(\mathbf{x},t)}$ is the velocity of the point with position $y^*(\mathbf{x},t)$ at time t. Hence, $\dot{u}(\mathbf{x},t)\mathbf{s}^*$ is the tangential velocity at time t of the material point at $\mathbf{y}^*$ relative to the material point at $\mathbf{x}$. In view of these definitions Coulomb's law of friction states that

$$\begin{array}{lllll} & |\tau| & \leq & 1 & \\ \text{and} & |\tau| & < & 1 & \text{implies} \quad \dot{u} = 0 \\ \text{while} & |\tau| & = & 1 & \text{implies} \quad \text{sign}(\dot{u}) = \text{sign}(\tau) \end{array} \tag{2.15}$$

In (2.15), $\dot{u} = 0$ means that the sticking condition is active, and so the tangential contact traction(t) is less than or is just reaching the frictional resistance$(\mu\lambda)$ at the contact surfaces. Also, $\dot{u} \neq 0$ means that the sliding condition is active. The condition gives $|t| = \mu\lambda$, that is, during motion, the magnitude of the tangential traction resisted by friction is $\mu\lambda$. The sliding motion continues as long as the frictional traction is developed to be equal to $\mu\lambda$. Once the developed tangential traction drops below the frictional capacity, the relative motion between the contactor and target

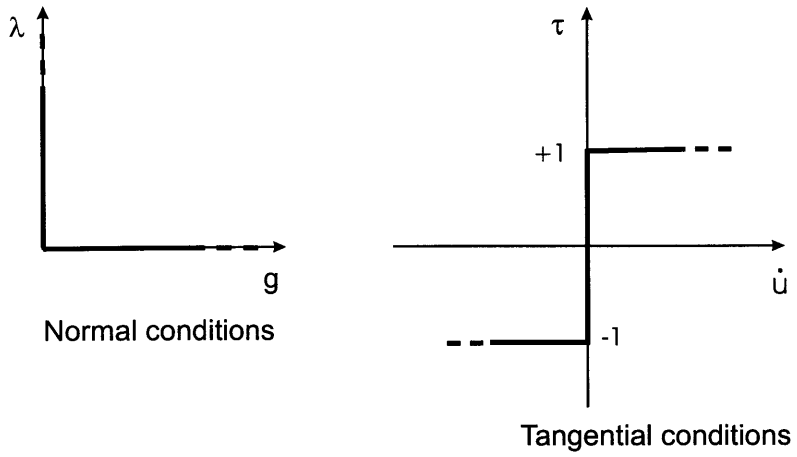

Figure 2-3: Interface conditions in contact analysis [1]

particles ceases (i.e., we have again sticking conditions), until such time that again the developed tangential traction is equal to the frictional capacity. According to the two conditions of sliding contact and sticking contact, we have $|\tau| \leq 1$.
In Figure(2-3), the left part illustrates the relations in equation(2.12) and the right part shows the relations in equation(2.15).

Hence, we can get the solution of the contact problem in Figure 2-1 by obtaining the solution of the virtual work equation (2.5) (specialized for bodies I and J) subject to the contact conditions, equations (2.12) and (2.15).

Chapter 3

Finite Element Solution Algorithms

3.1 Basic Solution Techniques

To impose contact constraints, two basic solution techniques can be used. These basic techniques are the *Lagrange multiplier method* and the *penalty method*. Based on the basic techniques, other technique, such as the *augmented Lagrangian method* can be derived and applied. In this section, we briefly review the basic techniques [1].

We consider a static mechanical problem subjected to discrete constraints. By using the standard finite element procedure, the discretized form can be obtained as follows:

$$\Pi = \frac{1}{2}\mathbf{U}^T\mathbf{K}\mathbf{U} - \mathbf{U}^T\mathbf{R} \tag{3.1}$$

$$\text{with the conditions} \quad \frac{\partial \Pi}{\partial \mathbf{U}} = 0 \tag{3.2}$$

where $\mathbf{U}$ is the global displacement vector, $\mathbf{K}$ the global stiffness matrix, and $\mathbf{R}$ the global load vector.

For the *Lagrange multiplier method*, if we subject (3.1) to the discrete constraints, $\mathbf{BU} = \mathbf{V}$ where $\mathbf{B}$ is a $m \times n$ matrix, the function to be minimized is replaced by the

following function:

$$\Pi^* = \frac{1}{2}\mathbf{U}^T\mathbf{K}\mathbf{U} - \mathbf{U}^T\mathbf{R} + \boldsymbol{\lambda}^T(\mathbf{B}\mathbf{U} - \mathbf{V}) \tag{3.3}$$

where $\boldsymbol{\lambda}$ is an unknown vector which contains m Lagrange multipliers and then we find $\mathbf{U}$ and $\boldsymbol{\lambda}$ by invoking stationarity of Π^*, i.e. $\delta\Pi^*$ is zero

$$\delta\Pi^* = \delta\mathbf{U}^T\mathbf{K}\mathbf{U} - \delta\mathbf{U}^T\mathbf{R} + \delta\boldsymbol{\lambda}^T(\mathbf{B}\mathbf{U} - \mathbf{V}) + \delta\mathbf{U}^T\mathbf{B}^T\boldsymbol{\lambda} = 0 \tag{3.4}$$

Using the fact that $\delta\mathbf{U}$ and $\delta\boldsymbol{\lambda}$ are arbitrary, we obtain

$$\left[\begin{array}{c|c} \mathbf{K} & \mathbf{B}^T \\ \hline \mathbf{B} & 0 \end{array}\right] \left[\begin{array}{c} \mathbf{U} \\ \hline \boldsymbol{\lambda} \end{array}\right] = \left[\begin{array}{c} \mathbf{R} \\ \hline \mathbf{V} \end{array}\right] \tag{3.5}$$

By solving (3.5), we obtain the displacements $\mathbf{U}$ and the Lagrange multipliers $\boldsymbol{\lambda}$. The elements in $\boldsymbol{\lambda}$ are interpreted as contacting forces at corresponding contacting nodes. Equilibrium equations (3.5) are the optimality conditions of the saddle point problem (see figure 3-1):

$$\inf_{\mathbf{u}} \sup_{\boldsymbol{\lambda}} \left\{\frac{1}{2}\mathbf{U}^T\mathbf{K}\mathbf{U} - \mathbf{U}^T\mathbf{R} + \boldsymbol{\lambda}^T\mathbf{B}\mathbf{U} - \boldsymbol{\lambda}^T\mathbf{V}\right\} \tag{3.6}$$

In figure 3-1, we can see that the minimum of $\Pi(u)$ subject to the constraint function is equal to the maximum of $-P(\lambda)$ and a point where they meet is a saddle point. In the figure, $-P(\lambda)$ is obtained as follows:

> we minimize Π^* in equation 3.3 with respect to $\mathbf{U}$. First, to show that Π^* is minimized at the finite soution $\mathbf{U}$, let us calculate Π^* at $\mathbf{U} + \boldsymbol{\varepsilon}$, where $\boldsymbol{\varepsilon}$ is any arbitrary vector,

$$\Pi^*|_{\mathbf{U}+\boldsymbol{\varepsilon}} = \frac{1}{2}(\mathbf{U}+\boldsymbol{\varepsilon})^T\mathbf{K}(\mathbf{U}+\boldsymbol{\varepsilon}) - (\mathbf{U}+\boldsymbol{\varepsilon})^T\mathbf{R} + \boldsymbol{\lambda}^T(\mathbf{B}(\mathbf{U}+\boldsymbol{\varepsilon}) - \mathbf{V})$$

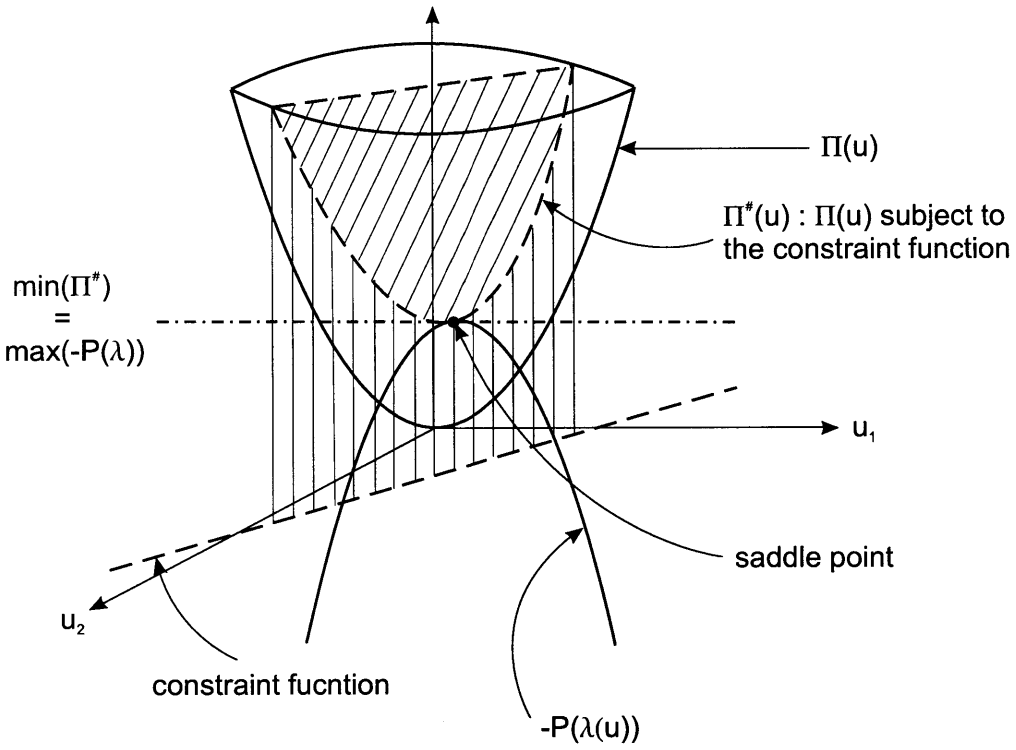

Figure 3-1: Saddle point problem

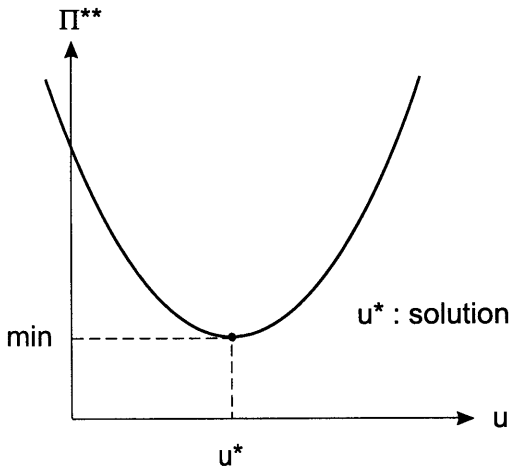

Figure 3-2: Minimum problem

$$
\begin{aligned}
&= \frac{1}{2}\mathbf{U}^T\mathbf{K}\mathbf{U} - \mathbf{U}^T\mathbf{R} + \boldsymbol{\lambda}^T(\mathbf{B}\mathbf{U} - \mathbf{V}) + \frac{1}{2}\boldsymbol{\varepsilon}^T\mathbf{K}\boldsymbol{\varepsilon} \\
&\quad + \boldsymbol{\varepsilon}(\mathbf{U}^T\mathbf{K} - \mathbf{R} + \boldsymbol{\lambda}^T\mathbf{B}) - \boldsymbol{\lambda}^T\mathbf{V} \\
&= \Pi^*|_{\mathbf{U}} + \frac{1}{2}\boldsymbol{\varepsilon}^T\mathbf{K}\boldsymbol{\varepsilon} + \boldsymbol{\varepsilon}(\mathbf{U}^T\mathbf{K} - \mathbf{R} + \boldsymbol{\lambda}^T\mathbf{B}) - \boldsymbol{\lambda}^T\mathbf{V} \qquad (3.7)
\end{aligned}
$$

where we used that $\mathbf{K}\mathbf{U} + \mathbf{B}^T\boldsymbol{\lambda} = \mathbf{R}$ and the fact that $\mathbf{K}$ is a symmetric matrix and a positive definite. Hence, $\Pi^*|_{\mathbf{U}}$ is the minimum of Π^*. The minimum of Π^* occurs when $\mathbf{U} = \mathbf{K}^{-1}(\mathbf{R} - \mathbf{B}^T\boldsymbol{\lambda})$, which is given by

$$
\begin{aligned}
\Pi^* &= -\frac{1}{2}(\mathbf{R} - \mathbf{B}^T\boldsymbol{\lambda})^T\mathbf{K}^{-1}(\mathbf{R} - \mathbf{B}^T\boldsymbol{\lambda}) - \boldsymbol{\lambda}^T\mathbf{V} \\
&= -\mathrm{P}(\boldsymbol{\lambda}) \qquad (3.8)
\end{aligned}
$$

where P represents the total potential energy and that energy is minimized at equilibrium. It means that $-P(\boldsymbol{\lambda})$ is maximized. Hence, Π^* is minimized with respect to $\mathbf{U}$ and at the same time it is maximized with respect to $\boldsymbol{\lambda}$.

In the *penalty method*, a penalty function is introduced as follows:

$$
\Pi_p = \frac{\alpha}{2}(\mathbf{B}\mathbf{U} - \mathbf{V})^T(\mathbf{B}\mathbf{U} - \mathbf{V}) \qquad (3.9)
$$

where α is a penalty parameter of large magnitude and then we use the following function

$$
\begin{aligned}
\Pi^{**} &= \Pi + \Pi_p \\
&= \frac{1}{2}\mathbf{U}^T\mathbf{K}\mathbf{U} - \mathbf{U}^T\mathbf{R} + \frac{\alpha}{2}(\mathbf{B}\mathbf{U} - \mathbf{V})^T(\mathbf{B}\mathbf{U} - \mathbf{V}) \qquad (3.10)
\end{aligned}
$$

To find the minimum of Π^{**} (see figure 3-2), we use $\delta\Pi^{**} = 0$, which gives

$$
\delta\Pi^{**} = \delta\mathbf{U}^T\mathbf{K}\mathbf{U} - \delta\mathbf{U}^T\mathbf{R} + \alpha\delta\mathbf{U}^T\mathbf{B}^T(\mathbf{B}\mathbf{U} - \mathbf{V}) = 0 \qquad (3.11)
$$

and obtain

$$
(\mathbf{K} + \alpha\mathbf{B}^T\mathbf{B})\mathbf{U} = \mathbf{R} + \alpha\mathbf{B}^T\mathbf{V} \qquad (3.12)
$$

The *Lagrange multiplier method* is often an effective procedure and the constraint condition is enforced "exactly", however, care must be taken that the stiffness matrix is non-singular. The *penalty method* is effective because no additional Lagrange multiplier equation is required but it has the drawback that it is sensitive to the choice of the penalty factor: a large penalty number leads to ill-conditioning of the global stiffness matrix whereas a small penalty number results in a non-negligible violation of the constraint conditions. The choice of the penalty factor can be difficult and is problem-dependent. Also, it is difficult to generalize this approach to large deformation sliding conditions.

In this context, the *augmented Lagrangian method* has been proposed as a procedure to partially overcome these difficulties. A combination of the *penalty* and the *Lagrange multiplier methods* leads to the *augmented Lagrangian method* as follows

$$\widetilde{\Pi}^* = \frac{1}{2}\mathbf{U}^T\mathbf{K}\mathbf{U} - \mathbf{U}^T\mathbf{R} + \frac{\alpha}{2}(\mathbf{B}\mathbf{U} - \mathbf{V})^T(\mathbf{B}\mathbf{U} - \mathbf{V}) + \lambda^T(\mathbf{B}\mathbf{U} - \mathbf{V}) \tag{3.13}$$

If we take $\delta\widetilde{\Pi}^* = 0$, which gives

$$\delta\widetilde{\Pi}^* = \delta\mathbf{U}^T\left[\mathbf{K}\mathbf{U} - \mathbf{R} + \alpha\mathbf{B}^T(\mathbf{B}\mathbf{U} - \mathbf{V}) + \mathbf{B}^T\lambda\right] + \delta\lambda^T(\mathbf{B}\mathbf{U} - \mathbf{V}) = 0 \tag{3.14}$$

we find that

$$\left[\begin{array}{c|c} \mathbf{K} + \alpha\mathbf{B}^T\mathbf{B} & \mathbf{B}^T \\ \hline \mathbf{B} & 0 \end{array}\right]\left[\begin{array}{c} \mathbf{U} \\ \hline \lambda \end{array}\right] = \left[\begin{array}{c} \mathbf{R} + \alpha\mathbf{B}^T\mathbf{V} \\ \hline \mathbf{V} \end{array}\right] \tag{3.15}$$

Augmented Lagrangian methods remove the requirement that the penalty parameter be large. In the above equation, we can find that when $\alpha = 0$, the equation reduces to equation (3.5).

Due to the difficulties to resolve the mechanical behavior in the contact interface, several different approaches have been used in the literature to solve contact problems. In Section 3.2 and 3.3, among those approaches, we describe two methods, the segment method [2] and the constraint function method [3] as finite element solution algorithms (which are implemented in the ADINA program).

3.2 The Segment Method

This method was suggested by K.J. Bathe and A. Chaudhary [2] as a contact solution algorithm. For the formulation of this algorithm, the incremental procedure and the notation presented in [1] are used.

This algorithm for contact solution has the following features:

- The kinematic conditions are enforced at the contactor nodes: To enforce the geometric compatibility conditions due to contact, a Lagrange multiplier procedure is used and the total potential of the contact forces is involved in the variational formulation.

- The frictional conditions are enforced over the contact segments: The state of a contact segment is determined using the segment resultant forces and Coulomb's law of friction and the conditions of adjoining segments are used to decide whether a surface node is in sticking contact, sliding contact or is releasing.

- In the contact area, the contact tractions are obtained from the externally applied forces and nodal point forces corresponding to the current element stresses.

- The number of Lagrange multiplier equations due to contact is dynamically adjusted in each iteration: If the node is in sticking contact, there are two equations for the node and if the node is in sliding contact, there is one equation for the node.

In numerical solutions, the contact surfaces (the contactor and target surface) are discretized by two-node linear segments and the contactor surface nodes are considered to come into contact with the target surface segments. If both nodes which are connected to a segment are in contact with the target surface, the contactor segment is defined to be in contact. In the contact area, the displacements and coordinates are interpolated linearly between adjacent nodes on the contact surfaces of the bodies by a location parameter(β). After the two bodies have come into contact, the incremental contactor surface displacements must be compatible with the incremental target

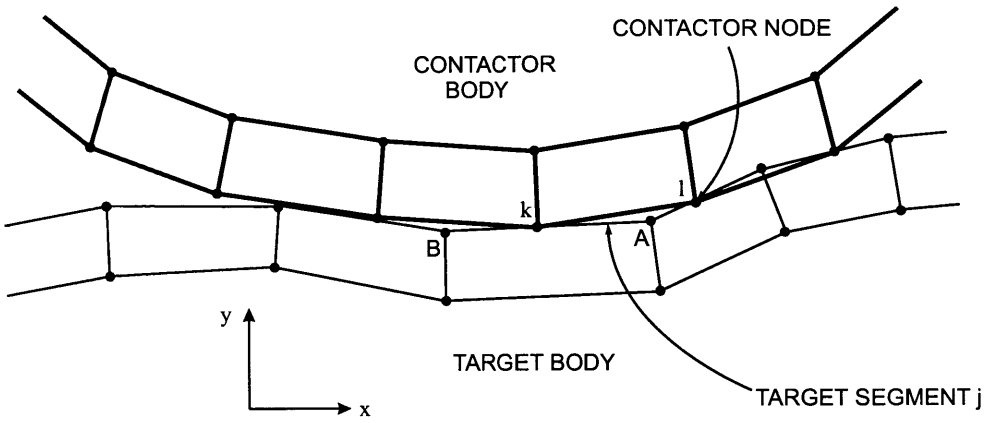

Figure 3-3: Finite element discretization in contact region [2]

surface displacements so that the current conditions of sticking contact and sliding contact between the contactor and target surfaces are satisfied. This compatibility of surface displacements is only enforced at the discrete locations corresponding to the contactor nodes. Hence, in an equilibrium configuration, the contactor nodes cannot be within the target body. (see Figure 3-3)

3.2.1 Potential of contact forces

In Section 3.1, we obtained the governing finite element equations by invoking stationarity of the total potential. In the case of contact problems, the functional is represented as follows:

$$\Pi_1 = \Pi - \sum_k W_k \tag{3.16}$$

where Π is the incremental total potential for generating equilibrium equations without contact conditions, and $\sum_k W_k$ is the incremental total potential of contact forces. In this section, more details about this term are discussed. As a preliminary for constructing the term, general geometric variables and contact forces in the contact area are introduced as shown in Figure 3-4 and 3-5. Figure 3-4 illustrates how the contactor node k comes into contact with the target segment j. Here, $\mathbf{\Delta}_k^{(i-1)}$ represents the material overlap which is eliminated in iteration (i) by the basic geometric

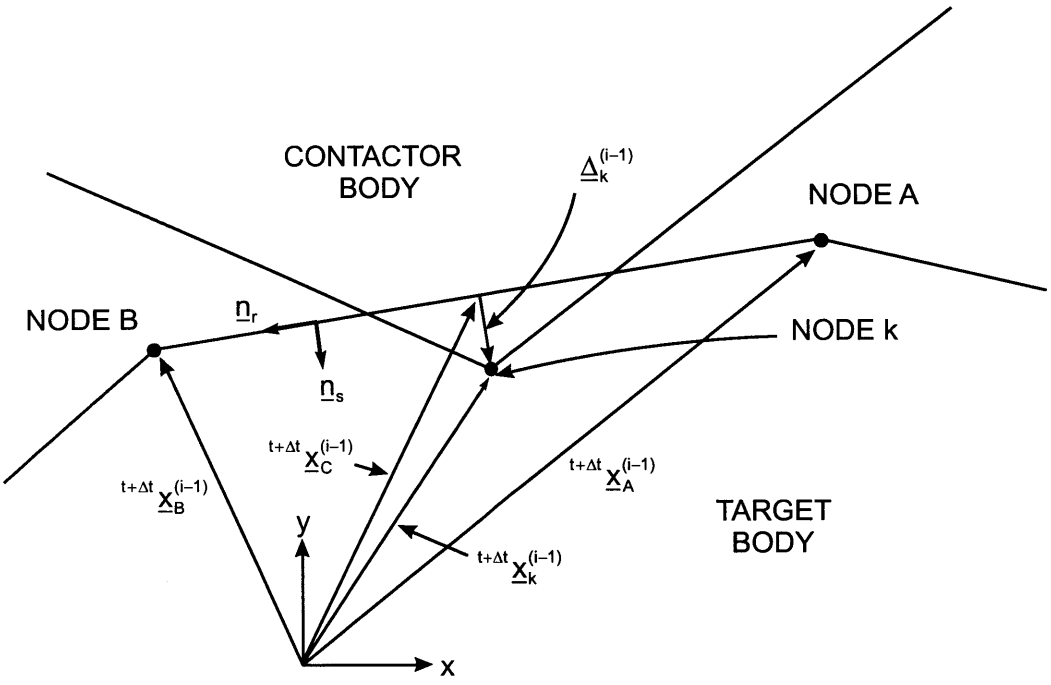

Figure 3-4: Definition of geometric variables [2]

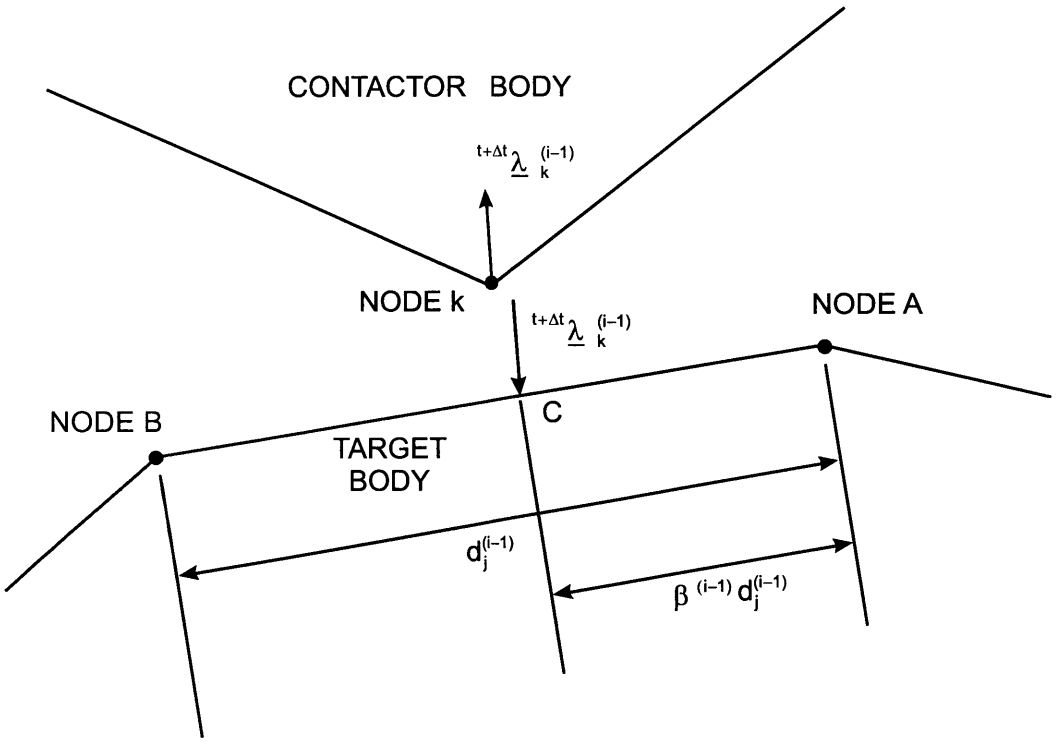

Figure 3-5: Contact forces [2]

condition of contact that no material overlap can occur between the bodies. From geometry, $\mathbf{\Delta}_k^{(i-1)}$ and $\beta^{(i-1)}$, which is the parameter of location of physical point of contact, are given by

$$\mathbf{\Delta}_k^{(i-1)} = {}^{t+\Delta t}\mathbf{x}_k^{(i-1)} - {}^{t+\Delta t}\mathbf{x}_C^{(i-1)} \tag{3.17}$$

$$\beta^{(i-1)} = \mathbf{n}_r^T \left[({}^{t+\Delta t}\mathbf{x}_k^{(i-1)} - \mathbf{\Delta}_k^{(i-1)}) - {}^{t+\Delta t}\mathbf{x}_A^{(i-1)} \right] \tag{3.18}$$

Then, in iteration (i), the following equation is satisfied

$${}^{t+\Delta t}\mathbf{x}_k^{(i)} = {}^{t+\Delta t}\mathbf{x}_C^{(i)} \tag{3.19}$$

For the constraint equation in sticking contact, the following manipulations are given. Subtracting ${}^{t+\Delta t}\mathbf{x}_C^{(i-1)}$ from both sides of equation (3.19),

$${}^{t+\Delta t}\mathbf{x}_k^{(i)} - {}^{t+\Delta t}\mathbf{x}_C^{(i-1)} = {}^{t+\Delta t}\mathbf{x}_C^{(i)} - {}^{t+\Delta t}\mathbf{x}_C^{(i-1)} \tag{3.20}$$

Then, using the relation of equation (3.17),

$${}^{t+\Delta t}\mathbf{x}_k^{(i)} - {}^{t+\Delta t}\mathbf{x}_k^{(i-1)} + \mathbf{\Delta}_k^{(i-1)} = \Delta\mathbf{u}_C^{(i)} \tag{3.21}$$

We have from the above equation,

$$\Delta\mathbf{u}_k^{(i)} + \mathbf{\Delta}_k^{(i-1)} = \Delta\mathbf{u}_C^{(i)} \tag{3.22}$$

where by an isoparametric interpolation using the location parameter($\beta^{(i-1)}$)

$$\Delta\mathbf{u}_C^{(i)} = (1-\beta^{(i-1)})\Delta\mathbf{u}_A^{(i)} + \beta^{(i-1)}\Delta\mathbf{u}_B^{(i)} \tag{3.23}$$

Hence, the constraint equation in sticking contact can be obtained by the combination of equation (3.22) and (3.23) as follows:

$$\left[(\Delta\mathbf{u}_k^{(i)} + \mathbf{\Delta}_k^{(i-1)}) - (1-\beta^{(i-1)})\Delta\mathbf{u}_A^{(i)} - \beta^{(i-1)}\Delta\mathbf{u}_B^{(i)} \right] = 0 \tag{3.24}$$

where $\Delta\mathbf{u}_k^{(i)}$, $\Delta\mathbf{u}_A^{(i)}$ and $\Delta\mathbf{u}_B^{(i)}$ are the displacement increments at nodes k, A and B, respectively.

In the case of sliding contact, in iteration i, the physical point (point C in figure 3-4) of contact with the target segment can change because its tangential force is equal to the frictional capacity. However, by assuming the amount of sliding to be small and through linearizing about the geometry after iteration $(i-1)$, the constraint equation can be obtained as follows:

$$(\mathbf{n}_s^T)\left[(\Delta\mathbf{u}_k^{(i)} + \boldsymbol{\Delta}_k^{(i-1)}) - (1-\beta^{(i-1)})\Delta\mathbf{u}_A^{(i)} - \beta^{(i-1)}\Delta\mathbf{u}_B^{(i)}\right] = 0 \qquad (3.25)$$

where $\mathbf{n}_s$ is the unit vector along the local direction s on the target segment with respect to the global reference frame.

Figure 3-5 shows the contact force at contactor node k and the reaction contact force at point C on the target segment j. By an isoparametric interpolation, the following equation is satisfied.

$$\begin{aligned} {}^{t+\Delta t}\boldsymbol{\lambda}_k^{(i-1)} &= -\,{}^{t+\Delta t}\boldsymbol{\lambda}_A^{(i-1)} - {}^{t+\Delta t}\boldsymbol{\lambda}_B^{(i-1)} \\ &= -(1-\beta^{(i-1)})\,{}^{t+\Delta t}\boldsymbol{\lambda}_k^{(i-1)} - \beta^{(i-1)}\,{}^{t+\Delta t}\boldsymbol{\lambda}_k^{(i-1)} \end{aligned} \qquad (3.26)$$

The total potential W_k for sticking contact is obtained by summing up the potential of a contact force at each node (e.g., k, A and B)

$$W_k = {}^{t+\Delta t}\boldsymbol{\lambda}_k^{(i)T}(\Delta\mathbf{u}_k^{(i)} + \boldsymbol{\Delta}_k^{(i-1)}) + {}^{t+\Delta t}\boldsymbol{\lambda}_A^{(i)T}\Delta\mathbf{u}_A^{(i)} + {}^{t+\Delta t}\boldsymbol{\lambda}_B^{(i)T}\Delta\mathbf{u}_B^{(i)} \qquad (3.27)$$

In iteration i, the contact force at the node k is given by,

$${}^{t+\Delta t}\boldsymbol{\lambda}_k^{(i)} = {}^{t+\Delta t}\boldsymbol{\lambda}_k^{(i-1)} + \Delta\boldsymbol{\lambda}_k^{(i)} \qquad (3.28)$$

where $\Delta\boldsymbol{\lambda}_k^{(i)}$ is the change in the contact force at node k and components of $\Delta\boldsymbol{\lambda}_k^{(i)}$ are Lagrange multipliers.

By substituting equations (3.26) and (3.28) into equation (3.27), the rearranged

equation of W_k can be obtained as follows:

$$\begin{aligned} W_k &= {}^{t+\Delta t}\boldsymbol{\lambda}_k^{(i-1)T}\left[(\Delta\mathbf{u}_k^{(i)} + \boldsymbol{\Delta}_k^{(i-1)}) - (1-\beta^{(i-1)})\Delta\mathbf{u}_A^{(i)} - \beta^{(i-1)}\Delta\mathbf{u}_B^{(i)}\right] \\ &+ \Delta\boldsymbol{\lambda}_k^{(i)T}\left[(\Delta\mathbf{u}_k^{(i)} + \boldsymbol{\Delta}_k^{(i-1)}) - (1-\beta^{(i-1)})\Delta\mathbf{u}_A^{(i)} - \beta^{(i-1)}\Delta\mathbf{u}_B^{(i)}\right] \end{aligned} \quad (3.29)$$

This potential is used for all contactor nodes which are in sticking contact and the second term in equation (3.29) reflects the constraints of sticking contact in the incremental equations of equilibrium.

Also, the total potential W_k for sliding contact is obtained as follows:

$$\begin{aligned} W_k &= {}^{t+\Delta t}\boldsymbol{\lambda}_k^{(i-1)T}\left[(\Delta\mathbf{u}_k^{(i)} + \boldsymbol{\Delta}_k^{(i-1)}) - (1-\beta^{(i-1)})\Delta\mathbf{u}_A^{(i)} - \beta^{(i-1)}\Delta\mathbf{u}_B^{(i)}\right] \\ &+ \Delta\boldsymbol{\lambda}_s^{(i)}\left\{-\mathbf{n}_s^T\left[(\Delta\mathbf{u}_k^{(i)} + \boldsymbol{\Delta}_k^{(i-1)}) - (1-\beta^{(i-1)})\Delta\mathbf{u}_A^{(i)} - \beta^{(i-1)}\Delta\mathbf{u}_B^{(i)}\right]\right\} \end{aligned} \quad (3.30)$$

where $\Delta\boldsymbol{\lambda}_s^{(i)}$ is the change in the magnitude of the normal component of ${}^{t+\Delta t}\boldsymbol{\lambda}_k^{(i-1)}$. This potential is used for all contactor nodes which are in sliding contact.

3.2.2 Governing finite element equations

The total potential including the potential of the contact forces with the constraints of compatible boundary displacements is obtained by substituting from equations (3.29) and (3.30) into equation (3.16). Then, by invoking stationarity, $\delta\Pi_1 = 0$, the governing finite element equations for iteration (i) are generated as follows:

$$\left\{\begin{bmatrix} {}^{t+\Delta t}\mathbf{K}^{(i-1)} & \mathbf{0} \\ \mathbf{0} & \mathbf{0} \end{bmatrix} + \left[{}^{t+\Delta t}\mathbf{K}_c^{(i-1)}\right]\right\}\begin{bmatrix} \Delta\mathbf{U}^{(i)} \\ \Delta\boldsymbol{\lambda}^{(i)} \end{bmatrix} = \begin{bmatrix} {}^{t+\Delta t}\mathbf{R} \\ \mathbf{0} \end{bmatrix} - \begin{bmatrix} {}^{t+\Delta t}\mathbf{F}^{(i-1)} \\ \mathbf{0} \end{bmatrix} + \begin{bmatrix} {}^{t+\Delta t}\mathbf{R}_c^{(i-1)} \\ {}^{t+\Delta t}\boldsymbol{\Delta}_c^{(i-1)} \end{bmatrix} \quad (3.31)$$

${}^{t+\Delta t}\mathbf{K}_c^{(i-1)}$, ${}^{t+\Delta t}\mathbf{R}_c^{(i-1)}$ and ${}^{t+\Delta t}\boldsymbol{\Delta}_c^{(i-1)}$ include all contributions for all surface nodes that belong to the contact region. For simplicity, these terms are considered below for a generic contact region consisting of the contactor node k and its target segment

j. The total effect of all contactor nodes can be obtained by summing the individual contributions using the direct stiffness method.

In equation (3.31), ${}^{t+\Delta t}\mathbf{K}_c^{(i-1)}$ is the contact stiffness matrix that includes the constraints of compatible surface displacements after iteration $(i-1)$. On the other hand, ${}^{t+\Delta t}\mathbf{K}^{(i-1)}$ is the usual tangent stiffness matrix. The calculation of ${}^{t+\Delta t}\mathbf{K}^{(i-1)}$, ${}^{t+\Delta t}\mathbf{R}$ and ${}^{t+\Delta t}\mathbf{F}^{(i-1)}$ can be performed by employing the usual procedures [1].
In sticking contact, ${}^{t+\Delta t}\mathbf{K}_c^{(i-1)}$ and the overlap vector ${}^{t+\Delta t}\boldsymbol{\Delta}_c^{(i-1)}$ can be obtained as follows from the second term in equation (3.29).

$$
{}^{t+\Delta t}\mathbf{K}_c^{(i-1)} = \left[\begin{array}{c|cc}
 & -1 & 0 \\
 & 0 & -1 \\
 & 1-\beta^{(i-1)} & 0 \\
\mathbf{0} & 0 & 1-\beta^{(i-1)} \\
 & \beta^{(i-1)} & 0 \\
 & 0 & \beta^{(i-1)} \\
\hline
\text{symmetric} & \multicolumn{2}{c}{\mathbf{0}}
\end{array}\right] \tag{3.32}
$$

$$
{}^{t+\Delta t}\boldsymbol{\Delta}_c^{(i-1)} = \begin{bmatrix} \Delta_{kx}^{(i-1)} \\ \Delta_{ky}^{(i-1)} \end{bmatrix} \tag{3.33}
$$

where the overlap is eliminated in iteration (i). The corresponding contact forces ${}^{t+\Delta t}\mathbf{R}_c^{(i-1)}$, i.e. the vector of updated contact forces after iteration $(i-1)$, is given from the first term in equation (3.29) as follows:

$$
{}^{t+\Delta t}\mathbf{R}_c^{(i-1)} = \begin{bmatrix} {}^{t+\Delta t}\lambda_{kx}^{(i-1)} \\ {}^{t+\Delta t}\lambda_{ky}^{(i-1)} \\ -(1-\beta^{(i-1)})\ {}^{t+\Delta t}\lambda_{kx}^{(i-1)} \\ -(1-\beta^{(i-1)})\ {}^{t+\Delta t}\lambda_{ky}^{(i-1)} \\ -\beta^{(i-1)}\ {}^{t+\Delta t}\lambda_{kx}^{(i-1)} \\ -\beta^{(i-1)}\ {}^{t+\Delta t}\lambda_{ky}^{(i-1)} \end{bmatrix} \tag{3.34}
$$

where ${}^{t+\Delta t}\mathbf{R}_c^{(i-1)}$ are calculated from $\Delta\mathbf{R}^{(i-1)}$ which is the vector of nodal point contact forces prior to updating (see Section 3.2.3).

The corresponding solution vector for iteration (i) is in detail as follows:

$$
\begin{bmatrix} \Delta\mathbf{U}^{(i)} \\ \Delta\boldsymbol{\lambda}^{(i)} \end{bmatrix} = \begin{bmatrix} \Delta\mathbf{u}_k^{(i)} \\ \Delta\mathbf{u}_A^{(i)} \\ \Delta\mathbf{u}_B^{(i)} \\ \Delta\boldsymbol{\lambda}_k^{(i)} \end{bmatrix} \tag{3.35}
$$

where $\Delta\boldsymbol{\lambda}^{(i)}$ is the vector of increments in contact forces in iteration (i).

In the case of sliding contact, ${}^{t+\Delta t}\mathbf{K}_c^{(i-1)}$, ${}^{t+\Delta t}\boldsymbol{\Delta}_c^{(i-1)}$ and the corresponding solution vector in equation (3.31) are

$$
\begin{bmatrix} \Delta\mathbf{U}^{(i)} \\ \Delta\boldsymbol{\lambda}^{(i)} \end{bmatrix} = \begin{bmatrix} \Delta\mathbf{u}_k^{(i)} \\ \Delta\mathbf{u}_A^{(i)} \\ \Delta\mathbf{u}_B^{(i)} \\ \Delta\lambda_s^{(i)} \end{bmatrix} \tag{3.36}
$$

$$
{}^{t+\Delta t}\boldsymbol{\Delta}_c^{(i-1)} = \begin{bmatrix} -n_{sx}\ \Delta_{kx}^{(i-1)} - n_{sy}\ \Delta_{ky}^{(i-1)} \end{bmatrix} \tag{3.37}
$$

$$
{}^{t+\Delta t}\mathbf{K}_c^{(i-1)} = \left[\begin{array}{c|c} & -n_{sx} \\ & -n_{sy} \\ & (1-\beta^{(i-1)})\, n_{sx} \\ \mathbf{0} & (1-\beta^{(i-1)})\, n_{sy} \\ & \beta^{(i-1)}\, n_{sx} \\ & \beta^{(i-1)}\, n_{sy} \\ \hline \text{symmetric} & \mathbf{0} \end{array}\right] \tag{3.38}
$$

As shown above, to enforce sticking contact, two individual equations are necessary to constrain the x and y incremental displacements of node k. However, in the case of sliding contact, only one constraint equation along the direction $\mathbf{n}_s$ is needed.

Using equation (3.31), the procedure of calculations performed in the contact solution is as follows for iteration (i) at time $t + \Delta t$:

- Evaluate the updated contact forces, ${}^{t+\Delta t}\mathbf{R}_c^{(i-1)}$ from $\Delta\mathbf{R}^{(i-1)}$ (for more detail, see Section 3.2.3).

- For each contactor node, determine the target segment using the current geometry after iteration $(i-1)$ and calculate the material overlap and the location parameter(β).

- Find whether any new contactor nodes have come into contact after iteration $(i-1)$

- Determine the states of contactor nodes for iteration (i) using the state of adjoining contactor segments (see Section 3.2.3).

- Assemble all matrices in equation (3.31) including the contact matrices ${}^{t+\Delta t}\mathbf{K}_c^{(i-1)}$ and ${}^{t+\Delta t}\mathbf{\Delta}_c^{(i-1)}$. Then solve to obtain the solution $\Delta\mathbf{U}^{(i)}$ and $\Delta\boldsymbol{\lambda}^{(i)}$.

3.2.3 Evaluation of contact forces and contact conditions

The appropriate matrices for the cases of sticking and sliding contact respectively are used in generating equation (3.31). This means that the algorithm has to determine which contact condition shall be applied to the system of equations. In solving contact problems, much difficulty lies in this aspect for a reliable and effective scheme. The state of the contactor segment can be decided in the procedure based on calculating the contact force at node k, ${}^{t+\Delta t}\lambda_k^{(i-1)}$ for which components appear in the vector ${}^{t+\Delta t}\mathbf{R}_c^{(i-1)}$. The procedure of calculating a contact force is described below (see figure 3-6).

1. After iteration $(i-1)$, the nodal point forces $\Delta\mathbf{R}^{(i-1)}$ can be obtained as follows

$$\Delta\mathbf{R}^{(i-1)} = {}^{t+\Delta t}\mathbf{F}^{(i-1)} - {}^{t+\Delta t}\mathbf{R} \tag{3.39}$$

   where ${}^{t+\Delta t}\mathbf{F}^{(i-1)}$ is the vector of nodal point forces equivalent to the element stresses and ${}^{t+\Delta t}\mathbf{R}$ is the vector of total applied forces, and so $\Delta\mathbf{R}^{(i-1)}$ is the out-of-balance force vector.

2. From $\Delta\mathbf{R}^{(i-1)}$ over segment j which is connected to the nodes k and $k+1$, the nodal point values of the segment tractions, $\mathbf{t}_j$ are given by the following equation

$$\Delta\mathbf{R}_j = \mathbf{G}\,\mathbf{t}_j \tag{3.40}$$

   where

$$\Delta\mathbf{R}_j = \begin{bmatrix} \Delta\mathbf{R}_x^k & \Delta\mathbf{R}_y^k \\ \Delta\mathbf{R}_x^{k+1} & \Delta\mathbf{R}_y^{k+1} \end{bmatrix} \qquad \mathbf{t}_j = \begin{bmatrix} t_x^k & t_y^k \\ t_x^{k+1} & t_y^{k+1} \end{bmatrix} \tag{3.41}$$

   where $\Delta\mathbf{R}_x^k$ is the x-component of the consistent nodal load at node k due to the distributed segment tractions over segment j only, and so the total force $\Delta\mathbf{R}_k^{(i-1)}$ at node k is the sum of the tractions acting over all segments adjoining

node k:

$$\mathbf{G} = h \frac{d_j}{6} \begin{bmatrix} 2 & 1 \\ 1 & 2 \end{bmatrix} \tag{3.42}$$

where $\mathbf{G}$ is the coefficient matrix for plane stress and plane strain analysis with uniform thickness h and d_j is the length of the contactor segment j (see the reference [2] for the case of axisymmetric analysis).

3. The components t_x^k, t_y^k and t_x^{k+1}, t_y^{k+1} are transformed to the normal and tangential segment tractions, t_n^k, t_t^k and t_n^{k+1}, t_t^{k+1} for calculation of the total resultant normal force, $\mathbf{T}_n^j$ and tangential force, $\mathbf{T}_t^j$ acting on segment j in plane stress and plane strain analysis.

$$\begin{aligned} \mathbf{T}_n^j &= h \frac{d_j^{(i-1)}}{2} (t_n^k + t_n^{k+1}) \\ \mathbf{T}_t^j &= h \frac{d_j^{(i-1)}}{2} (t_t^k + t_t^{k+1}) \end{aligned} \tag{3.43}$$

4. Coulomb's law of friction, $\mathbf{T}_f^j = \mu \mathbf{T}_n^j$ is used to determine if the segment is in the sticking condition or sliding condition and the tangential segment traction is accordingly updated to $\tilde{t}_t$.

   - If $\mathbf{T}_f^j \geq |\mathbf{T}_t^j|$, the segment is in the sticking condition. In this case, $\tilde{t}_t = t_t$ and the updated nodal point forces $\Delta\tilde{\mathbf{R}}_j = \Delta\mathbf{R}_j$. The sum of contributions from updated tractions adjoining node k generates the total updated force ${}^{t+\Delta t}\boldsymbol{\lambda}_k^{(i-1)}$

   - If $\mathbf{T}_f^j < |\mathbf{T}_t^j|$, the segment is in the sliding condition. In this case, the total tangential force is scaled down to equal the frictional capacity and using this force, ${}^{t+\Delta t}\boldsymbol{\lambda}_k^{(i-1)}$ is generated.

5. According to the state of adjoining contactor segments, the state of a contactor node is decided as follows.

   - If one of two adjoining segments is sticking, the state of the contactor node

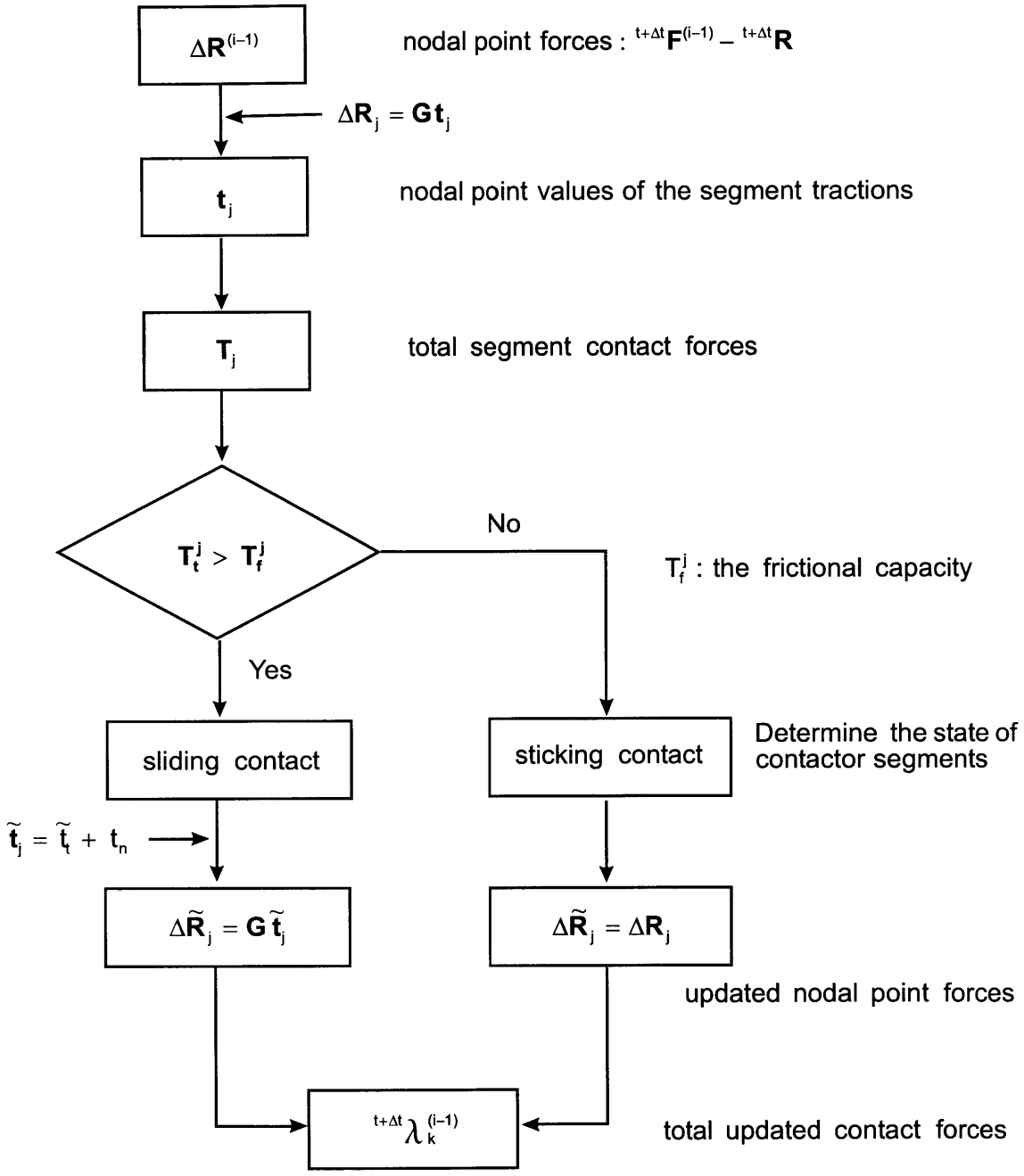

Figure 3-6: The procedure of calculation of contact forces

is sticking and if both adjoining segments are in the sliding condition, the state of the contactor node is sliding.

3.3 The Constraint Function Method

This method was suggested by Eterovic and Bathe [1] [3]. To apply the segment method to contact problems, it is necessary to adopt an active set strategy, in which only the equations corresponding to active constraints are included in each iteration. Hence, this feature may worsen the convergence properties of a full Newton-Raphson scheme if there are frequent changes of the active set.

The constraint function method enforces the contact and friction inequality constraints explicitly by means of appropriate constraint functions and does not require an active set procedure. This method is especially suitable for nonconservative problems like inelastic large-strain analysis with frictional conditions and it is based on the general equilibrium equations and contact conditions prescribed in Chapter 2.

In this method, the conditions to be satisfied are given in equations (2.12) and (2.15) and two constraint functions are defined, in which one is the normal constraint function $w(g, \lambda)$ and the other is the frictional constraint function $v(\dot{u}, \tau)$.

The following normal constraint function $w(g, \lambda)$ is used such that when $w(g, \lambda) = 0$, the conditions in (2.12) are satisfied

$$w(g, \lambda) = \frac{g + \lambda}{2} - \sqrt{\left(\frac{g - \lambda}{2}\right)^2 + \epsilon_n} \tag{3.44}$$

where the variables g, λ are the gap function and the normal traction component, respectively, and ϵ_n is a small parameter ($\epsilon_n \ll 1$).

In the case of friction, the conditions (2.15) are also satisfied when $v(\dot{u}, \tau) = 0$. To construct the constraint function, the following relationship is used

$$\tau = \frac{2}{\pi} \arctan \frac{\dot{u}}{\epsilon_t} \tag{3.45}$$

where ϵ_t is a small parameter ($\epsilon_t \ll 1$) which represents the characteristic behavior of the friction law.

Considering the variables λ and τ as Lagrange multipliers, the constraint equation for the continuum is as follows

$$\int_{S^{IJ}} [\delta\lambda \; w(g,\lambda) \; + \; \delta\tau \; v(\dot{u},\tau)] \; dS^{IJ} \; = \; 0 \tag{3.46}$$

where $\delta\lambda$ and $\delta\tau$ are variations.

For the two-body contact problem in figure 3-5, the constraint function method now consists of solving equation (2.5) and enforcing the following conditions

$$w(g,\lambda) \; = \; 0 \tag{3.47}$$

$$v(\dot{u},\tau) \; = \; 0 \tag{3.48}$$

The finite element solution of the governing continuum mechanics equation is achieved by using the usual discretization schemes.

The discretization of the governing equations (2.5) and (3.46) for the continuum at time $t + \Delta t$ is given by

$${}^{t+\Delta t}\mathbf{F}({}^{t+\Delta t}\mathbf{U}) \; = \; {}^{t+\Delta t}\mathbf{R} \; - \; {}^{t+\Delta t}\mathbf{R}_c({}^{t+\Delta t}\mathbf{U}, \; {}^{t+\Delta t}\boldsymbol{\tau}) \tag{3.49}$$

$${}^{t+\Delta t}\mathbf{F}_c({}^{t+\Delta t}\mathbf{U}, \; {}^{t+\Delta t}\boldsymbol{\tau}) \; = \; \mathbf{0} \tag{3.50}$$

where ${}^{t+\Delta t}\mathbf{U}$ is the vector of all unknown nodal point displacements, ${}^{t+\Delta t}\mathbf{F}({}^{t+\Delta t}\mathbf{U})$ is the vector of internal nodal point forces, ${}^{t+\Delta t}\mathbf{R}$ is the vector of external nodal point forces and with m contactor nodes ${}^{t+\Delta t}\boldsymbol{\tau}^T$ is given by

$${}^{t+\Delta t}\boldsymbol{\tau}^T \; = \; [\lambda_1, \tau_1, \ldots, \lambda_k, \tau_k, \ldots, \lambda_m, \tau_m] \tag{3.51}$$

The contact traction term in equation (2.5) will result into nodal point forces ${}^{t+\Delta t}\mathbf{R}_c$. The vector ${}^{t+\Delta t}\mathbf{R}_c$ is obtained by assembling for all m contactor nodes ($k = 1, \ldots, m$), the contactor nodal force vector ${}^{t+\Delta t}\mathbf{R}_k^c$ due to contact. ${}^{t+\Delta t}\mathbf{R}_k^c$ is given by

$$
{}^{t+\Delta t}\mathbf{R}_k^c = \begin{bmatrix} \lambda_k(\mathbf{n}_s + \mu\tau_k\mathbf{n}_r) \\ -(1-\beta_k)\lambda_k(\mathbf{n}_s + \mu\tau_k\mathbf{n}_r) \\ -\beta_k\lambda_k(\mathbf{n}_s + \mu\tau_k\mathbf{n}_r) \end{bmatrix} \tag{3.52}
$$

where $\beta_k, \mathbf{n}_s, \mathbf{n}_r$ are defined in figure 3-4 and 3-5, the first row term of ${}^{t+\Delta t}\mathbf{R}_k^c$ corresponds to the contactor node k and the second and third terms correspond to the target nodes A and B, respectively in figure 3-5.

The vector ${}^{t+\Delta t}\mathbf{F}_c$ in equation (3.50) can be written as

$$
{}^{t+\Delta t}\mathbf{F}_c^T = \left[{}^{t+\Delta t}\mathbf{F}_1^{c^T}, \ldots, {}^{t+\Delta t}\mathbf{F}_m^{c^T} \right] \tag{3.53}
$$

where

$$
{}^{t+\Delta t}\mathbf{F}_k^c = \begin{bmatrix} w(g_k, \lambda_k) \\ v(\dot{u}, \tau_k) \end{bmatrix} \tag{3.54}
$$

The incremental equations for solution of equations (3.49) and (3.50) are obtained by linearization about the last calculated state. Using the usual procedures [1], the incremental equations corresponding to the linearization about the state at time t are given by

$$
\begin{bmatrix} ({}^t\mathbf{K} + {}^t\mathbf{K}_{uu}^c) & {}^t\mathbf{K}_{u\tau}^c \\ {}^t\mathbf{K}_{\tau u}^c & {}^t\mathbf{K}_{\tau\tau}^c \end{bmatrix} \begin{bmatrix} \Delta\mathbf{U} \\ \Delta\boldsymbol{\tau} \end{bmatrix} = \begin{bmatrix} {}^t\mathbf{R} - {}^t\mathbf{F} - {}^t\mathbf{R}_c \\ -{}^t\mathbf{F}_c \end{bmatrix} \tag{3.55}
$$

where the matrix ${}^t\mathbf{K}$ is the usual tangent stiffness matrix not including contact conditions, $\Delta\mathbf{U}$ and $\Delta\boldsymbol{\tau}$ are the increments, and ${}^t\mathbf{K}_{uu}^c, {}^t\mathbf{K}_{u\tau}^c, {}^t\mathbf{K}_{\tau u}^c, {}^t\mathbf{K}_{\tau\tau}^c$ represent contact stiffness matrices, which are given by

$$
\begin{aligned}
{}^t\mathbf{K}^c_{uu} &= \frac{\partial^t \mathbf{R}_c}{\partial^t \mathbf{U}}; \qquad & {}^t\mathbf{K}^c_{u\tau} &= \frac{\partial^t \mathbf{R}_c}{\partial^t \boldsymbol{\tau}} \\
{}^t\mathbf{K}^c_{\tau u} &= \frac{\partial^t \mathbf{F}_c}{\partial^t \mathbf{U}}; \qquad & {}^t\mathbf{K}^c_{\tau\tau} &= \frac{\partial^t \mathbf{F}_c}{\partial^t \boldsymbol{\tau}}
\end{aligned} \tag{3.56}
$$

Due to the presence of friction the system matrix in equation (3.55) is in general nonsymmetric but for frictionless contact, a symmetric matrix is obtained.

It is important to note that although the incremental equations (3.55) correspond to a full linearization, the solution may be sensitive to the choice of time stepping, that is, when too large incremental time steps are used, convergence difficulties in the equilibrium iterations may occur. In general, large time steps can only be taken when not much change in the sticking and sliding regions is expected.

Chapter 4

Numerical Solutions

4.1 Mooney-Rivlin Material Behavior

In the numerical solutions, we shall use the rubber material, especially the Mooney-Rivlin material model which is also available in ADINA. In this section, we briefly discuss this material model.

The conventional Mooney-Rivlin material model [1] is represented by the strain energy density per unit original volume as follows.

$$ {}^t_0\tilde{W} = C_1({}^t_0I_1 - 3) + C_2({}^t_0I_2 - 3); \qquad {}^t_0I_3 = 1 \tag{4.1} $$

where ${}^t_0\tilde{W}$ is the strain energy density, C_1 and C_2 are material constants and the ${}^t_0I_i$ are the invariants given in terms of the components of the Cauchy-Green deformation tensor(${}^t_0\mathbf{C}$) as below

$$ \begin{aligned} {}^t_0I_1 &= {}^t_0C_{kk} \\ {}^t_0I_2 &= \frac{1}{2}\left[({}^t_0I_1)^2 - {}^t_0C_{ij}\ {}^t_0C_{ij}\right] \\ {}^t_0I_3 &= \det {}^t_0\mathbf{C} \end{aligned} \tag{4.2} $$

We consider the one-dimensional response of a bar (assume the section is a square) as shown in figure 4-1 and examine the force-displacement relationship for $C_1 = 0.293$

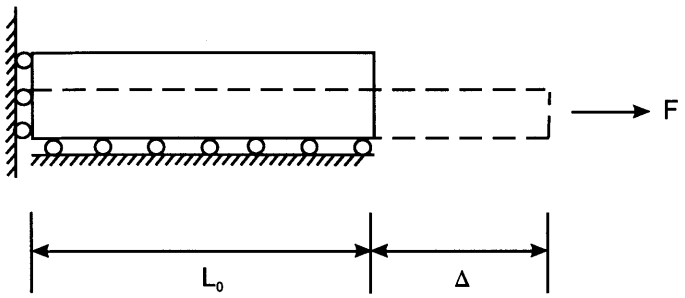

Figure 4-1: One-dimensional rubber bar

and $C_2 = 0.177$.

We can start using ${}^t_0S_{ij} = \partial\, {}^t_0\tilde{W}/\partial\, {}^t_0\epsilon_{ij}$ as follows

$$ {}^t_0S_{11} = \frac{\partial\, {}^t_0\tilde{W}}{\partial\, {}^t_0\epsilon_{11}} = C_1\frac{\partial\, {}^t_0I_1}{\partial\, {}^t_0\epsilon_{11}} + C_2\frac{\partial\, {}^t_0I_2}{\partial\, {}^t_0\epsilon_{11}} \tag{4.3} $$

where ${}^t_0S_{11}$ is the second Piola-Kirchhoff stress and ${}^t_0\epsilon_{11}$ is the Green-Lagrange strain. With the fact that after and before deformation, this model should have the same volume, we can obtain the deformation gradient(${}^t_0\mathbf{X}$), the Cauchy-Green deformation tensor(${}^t_0\mathbf{C}$) and the Green-Lagrange strain(${}^t_0\boldsymbol{\epsilon}$).

$$ {}^t_0\mathbf{X} = \begin{bmatrix} \lambda & 0 & 0 \\ 0 & \frac{1}{\sqrt{\lambda}} & 0 \\ 0 & 0 & \frac{1}{\sqrt{\lambda}} \end{bmatrix}, \quad {}^t_0\mathbf{C} = {}^t_0\mathbf{X}^T\, {}^t_0\mathbf{X} = \begin{bmatrix} \lambda^2 & 0 & 0 \\ 0 & \frac{1}{\lambda} & 0 \\ 0 & 0 & \frac{1}{\lambda} \end{bmatrix} $$

$$ {}^t_0\boldsymbol{\epsilon} = \frac{1}{2}({}^t_0\mathbf{C} - \mathbf{I}) = \frac{1}{2}\begin{bmatrix} (\lambda^2 - 1) & 0 & 0 \\ 0 & (\frac{1}{\lambda} - 1) & 0 \\ 0 & 0 & (\frac{1}{\lambda} - 1) \end{bmatrix} \tag{4.4} $$

where $\lambda = 1 + \Delta/L_0$

By using the chain rule, $\partial\,{}^t_0I_1/\partial\,{}^t_0\epsilon_{11}$ and $\partial\,{}^t_0I_2/\partial\,{}^t_0\epsilon_{11}$ is given by

$$\frac{\partial\,{}^t_0I_1}{\partial\,{}^t_0\epsilon_{11}} = \frac{\partial\,{}^t_0I_1}{\partial\,{}^t_0C_{11}}\frac{\partial\,{}^t_0C_{11}}{\partial\,{}^t_0\epsilon_{11}} + \frac{\partial\,{}^t_0I_1}{\partial\,{}^t_0C_{22}}\frac{\partial\,{}^t_0C_{22}}{\partial\,{}^t_0\epsilon_{11}} + \frac{\partial\,{}^t_0I_1}{\partial\,{}^t_0C_{33}}\frac{\partial\,{}^t_0C_{33}}{\partial\,{}^t_0\epsilon_{11}}$$

$$= 2(1 - \frac{1}{\lambda^3}) \tag{4.5}$$

$$\frac{\partial\,{}^t_0I_2}{\partial\,{}^t_0\epsilon_{11}} = \frac{\partial\,{}^t_0I_2}{\partial\,{}^t_0C_{11}}\frac{\partial\,{}^t_0C_{11}}{\partial\,{}^t_0\epsilon_{11}} + \frac{\partial\,{}^t_0I_2}{\partial\,{}^t_0C_{22}}\frac{\partial\,{}^t_0C_{22}}{\partial\,{}^t_0\epsilon_{11}} + \frac{\partial\,{}^t_0I_2}{\partial\,{}^t_0C_{33}}\frac{\partial\,{}^t_0C_{33}}{\partial\,{}^t_0\epsilon_{11}}$$

$$= 2(\frac{1}{\lambda} - \frac{1}{\lambda^4}) \tag{4.6}$$

Hence, we can obtain ${}^t_0S_{11}$ by substituting from equations (4.5) and (4.6) into equation (4.3) as follows

$${}^t_0S_{11} = 2\left[C_1(1 - \frac{1}{\lambda^3}) + C_2(\frac{1}{\lambda} - \frac{1}{\lambda^4})\right] \tag{4.7}$$

and the Cauchy stress tensor(${}^t\boldsymbol{\tau}$) can be given in terms of the second Piola-Kirchhoff stress tensor as follows.

$${}^t\boldsymbol{\tau} = \frac{{}^t\rho}{{}_0\rho}\,{}^t_0\mathbf{X}\,{}^t_0\mathbf{S}\,{}^t_0\mathbf{X}^T \tag{4.8}$$

Then, using equation (4.7) and (4.8), we can obtain the force-displacement relationship [1], which is given by

$$F = 2\,{}^0\mathrm{A}\left[C_1(\lambda - \frac{1}{\lambda^2}) + C_2(1 - \frac{1}{\lambda^3})\right] \tag{4.9}$$

where ^{0}A is the original cross-section of the bar.

Figure 4-2 shows the force-displacement curve specialized to $C_1 = 0.293$ and $C_2 = 0.177$. We can find that as the displacement increases in the compression part, the stiffness of the rubber bar increases more drastically than in the tension part.

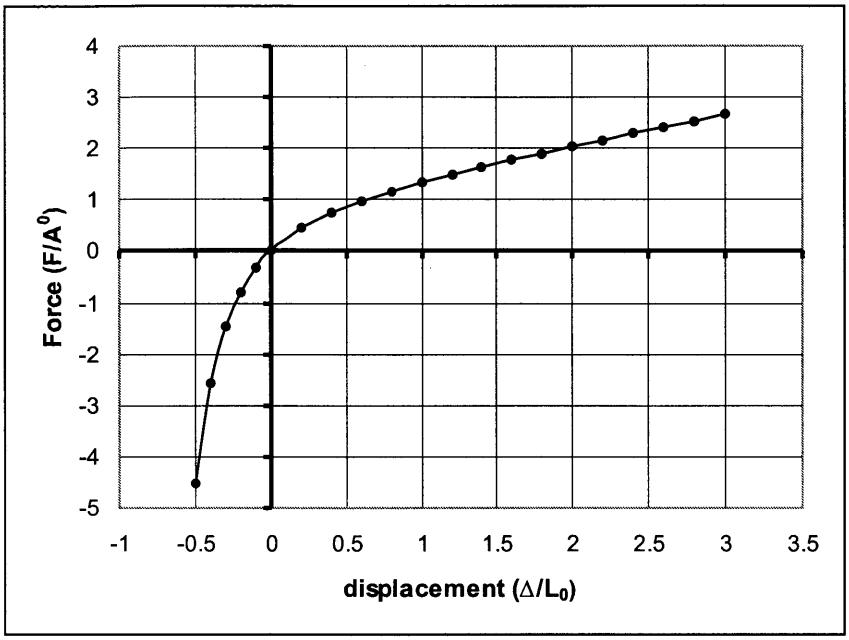

Figure 4-2: The force-displacement curve for the rubber bar

4.2 Example 1 - Analysis of Rectangular Rubber Block

Figure 4-3 shows the rectangular rubber block considered. A long rectangular block of size $1.0m \times 1.0m$ is analyzed; hence in this model plane strain conditions are assumed. The rigid target surface is modelled by specifying nodes with no degrees of freedom. We idealize the piece of rubber using a Mooney-Rivlin description, with $C_1 = 0.293MPa$, $C_2 = 0.177MPa$ and $\kappa = 1410MPa$. In this example, 4/1 elements and 9/3 elements are used and their solutions are compared to each other and in each case, five finite element meshes are used (4×4, 8×8, 16×16, 32×32 and 64×64 meshes). The load is applied by prescribing the displacements at the top of the mesh and both, moderate displacements ($\Delta = 0.1m$) and large displacements ($\Delta = 0.5m$) are considered. We also examine two cases, namely, assuming no friction and friction ($\mu = 0.3$) between the contactor surface and the target surface of this model. The load (displacement, Δ) is applied in ten equal load steps.

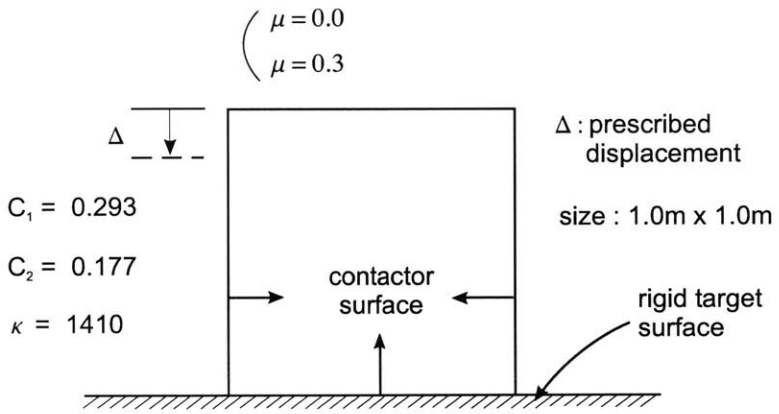

Figure 4-3: Rectangular rubber block

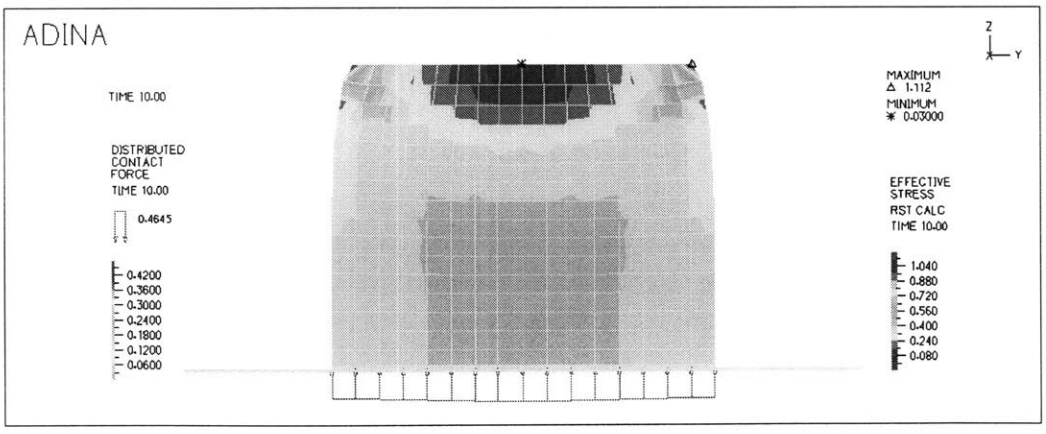

Figure 4-4: Effective stress and distributed contact force for the rectangular rubber block (4/1 elements with no friction, 16 × 16 mesh)

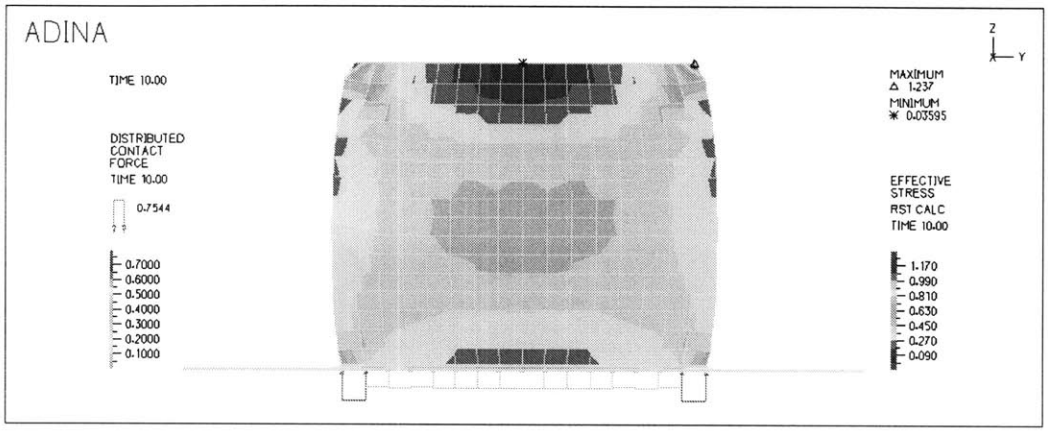

Figure 4-5: Effective stress and distributed contact force for the rectangular rubber block (4/1 elements with friction, 16×16 mesh)

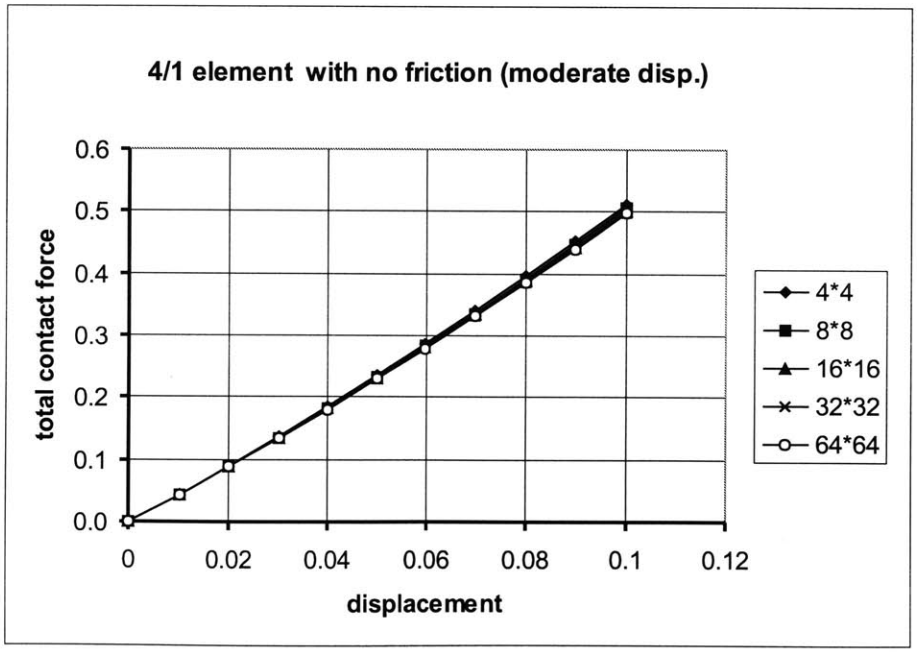

Figure 4-6: Force-displacement curve for the rectangular rubber block, $\Delta = 0.1m$ (4/1 elements with no friction)

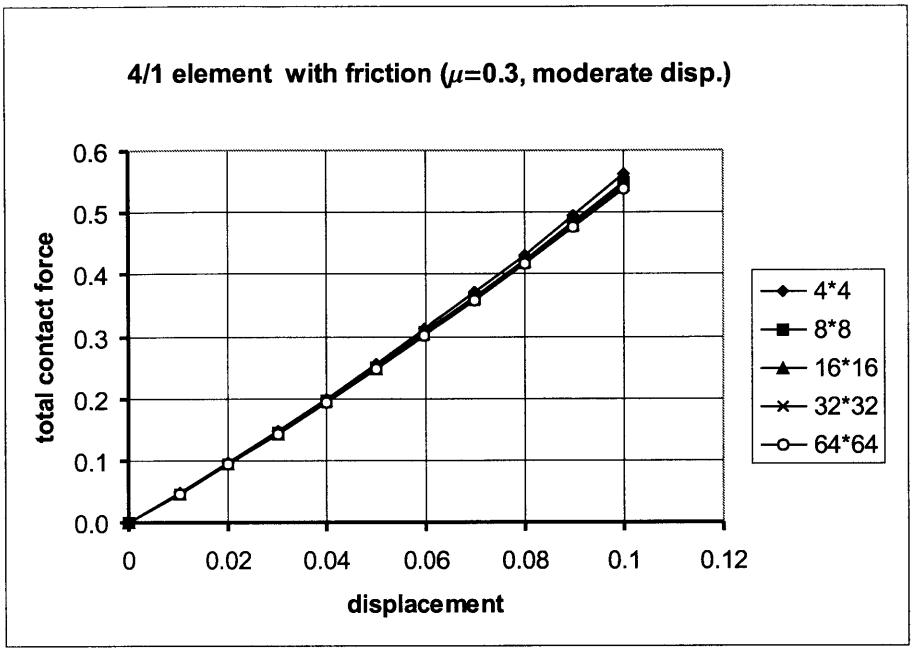

Figure 4-7: Force-displacement curve for the rectangular rubber block, $\Delta = 0.1m$ (4/1 elements with friction)

First, we consider moderate displacements. Figures 4-4 and 4-5 show the effective stress and distributed contact force in the case of the 16×16 mesh for both cases with no friction and friction ($\mu = 0.3$). As shown in the figures, in the case of friction, a concentration of distributed contact force in both bottom edge elements of the model is developed. The concentration is caused by frictional resistance. Figures 4-6 and 4-7 show the force-displacement curves in both cases with no friction and friction ($\mu = 0.3$) using 4/1 elements. In these figures, both curves represent similar patterns but we see that the case with friction results in a larger total contact force than the case with no friction. This means that the effects of friction make the model stiffer. Figure 4-8 shows the force-displacement curve using 9/3 elements. The figure shows that the five finite element solutions are in close agreement with the 4/1 element solutions.

For the large displacement solutions, the resulting force-displacement curves are shown in figure 4-9 for the 4/1 elements and figure 4-10 for the 9/3 elements. In

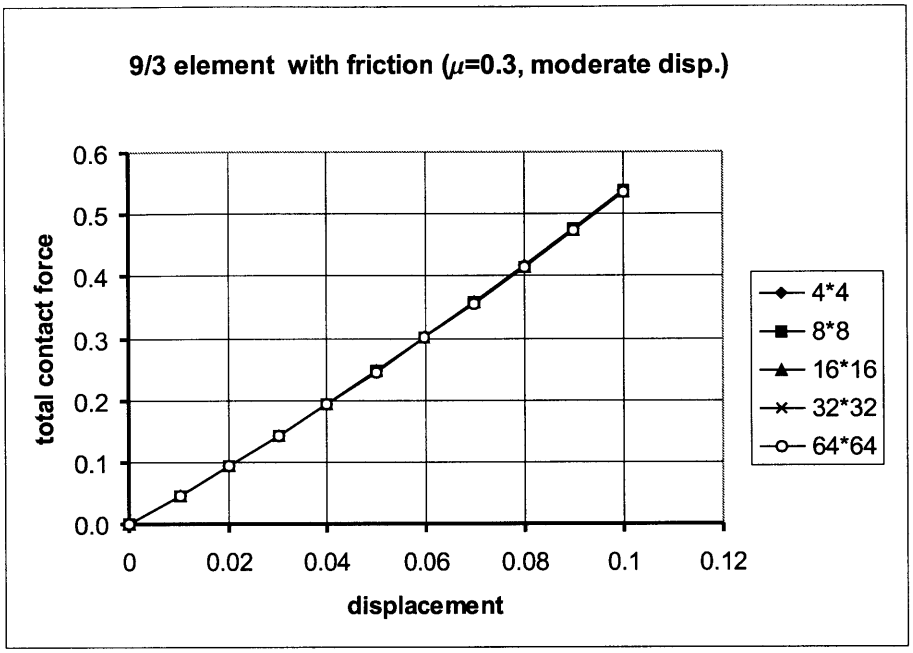

Figure 4-8: Force-displacement curve for the rectangular rubber block, $\Delta = 0.1m$ (9/3 elements with friction)

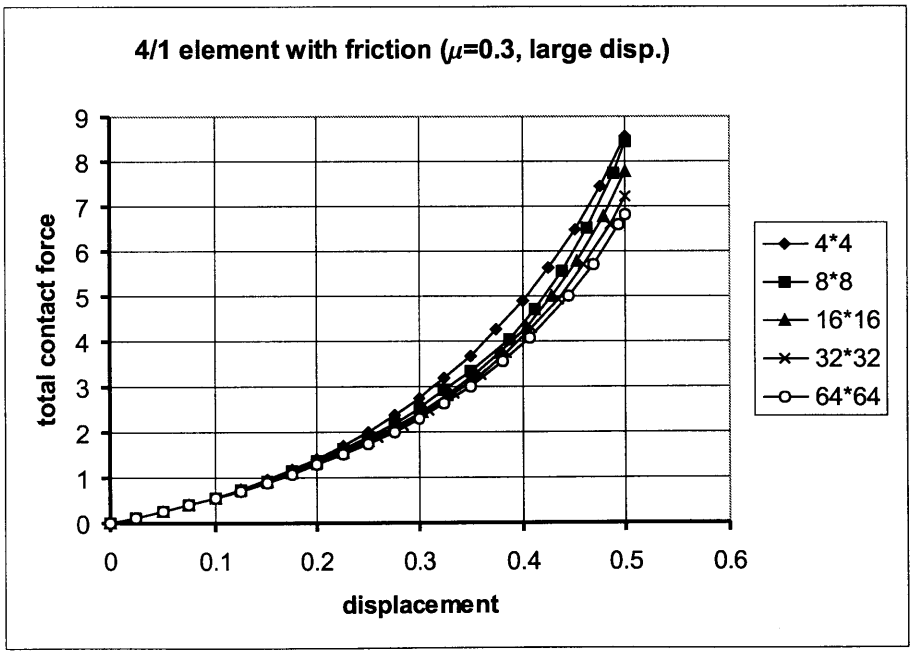

Figure 4-9: Force-displacement curve for the rectangular rubber block, $\Delta = 0.5m$ (4/1 elements with friction)

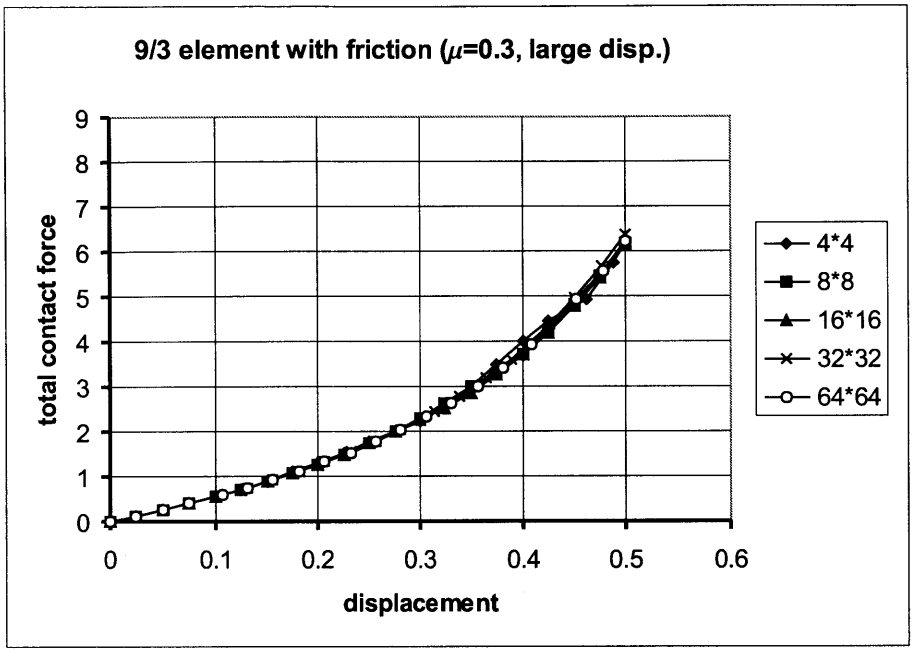

Figure 4-10: Force-displacement curve for the rectangular rubber block, $\Delta = 0.5m$ (9/3 elements with friction)

figure 4-9, we can see that as the size of the elements becomes smaller, the total contact forces decrease. The results agree with the observation that in general finite solutions, coarser meshes are stiffer than finer meshes. In the case of the 9/3 elements, the curves do not show the general pattern as in the case of the 4/1 elements but the five finite element solutions are also in close agreement as in the case of moderate displacements. We note that the 9/3 element is much more powerful in this analysis, namely the 4×4 mesh gives already good results (whereas a 64×64 mesh of 4/1 elements must be used).

4.3 Example 2 - Analysis of Cylindrical Rubber Block

In this example, a cylindrical rubber block with radius R=0.5m is analyzed and plane strain conditions are also assumed. To model the contactor, the same elements (4/1

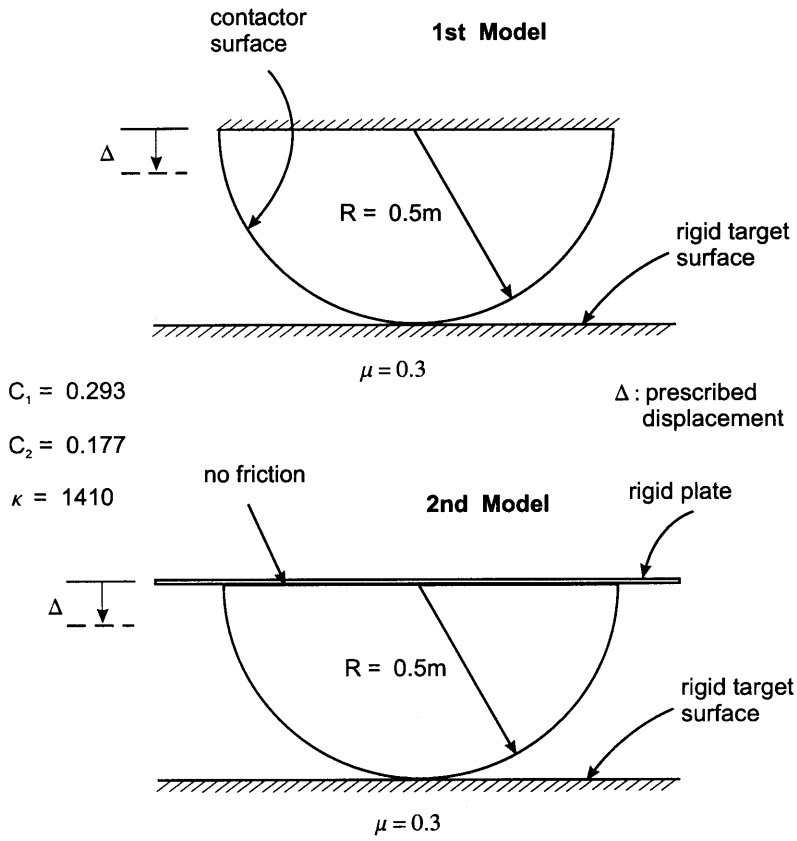

Figure 4-11: Cylindrical rubber block

elements and 9/3 elements) are used as in Section 4.2 and in each case, we also examine the performance of the five finite element meshes (4×4, 8×8, 16×16, 32×32 and 64×64 meshes). Figure 4-12 shows the finite element idealization of the 8×8 mesh.

The rigid target surface is also modelled by specifying nodes with no degrees of freedom. Here, we use two analysis models, the 1st model and the 2nd model (see figure 4-11). The 1st model is used for moderate displacements and the 2nd model is used for both moderate and large displacement conditions because when the 1st model is used for large displacements, the solution fails to converge due to distorted elements. In both cases, the friction coefficient $\mu = 0.3$ is used between the contactor surface and the target surface. We idealize the piece of rubber with the same material constants as in the above example. Both moderate displacement ($\Delta = 0.05m$) and large

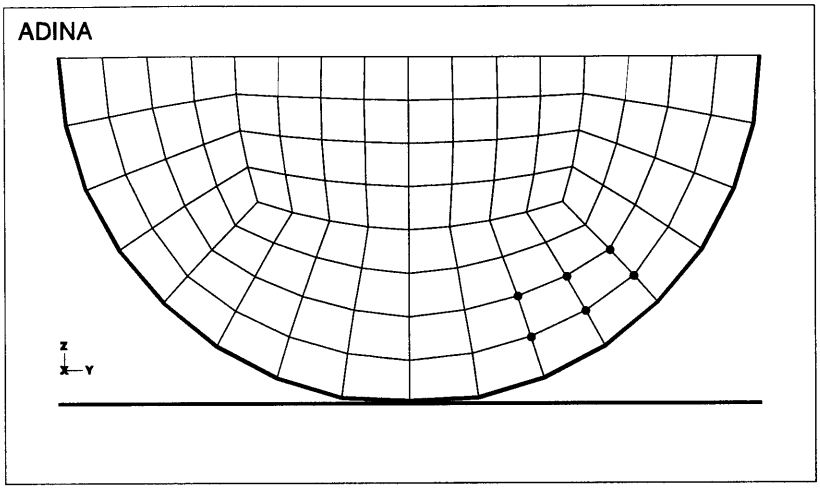

Figure 4-12: Mesh used for the cylindrical rubber block (4/1 elements, 8×8 mesh)

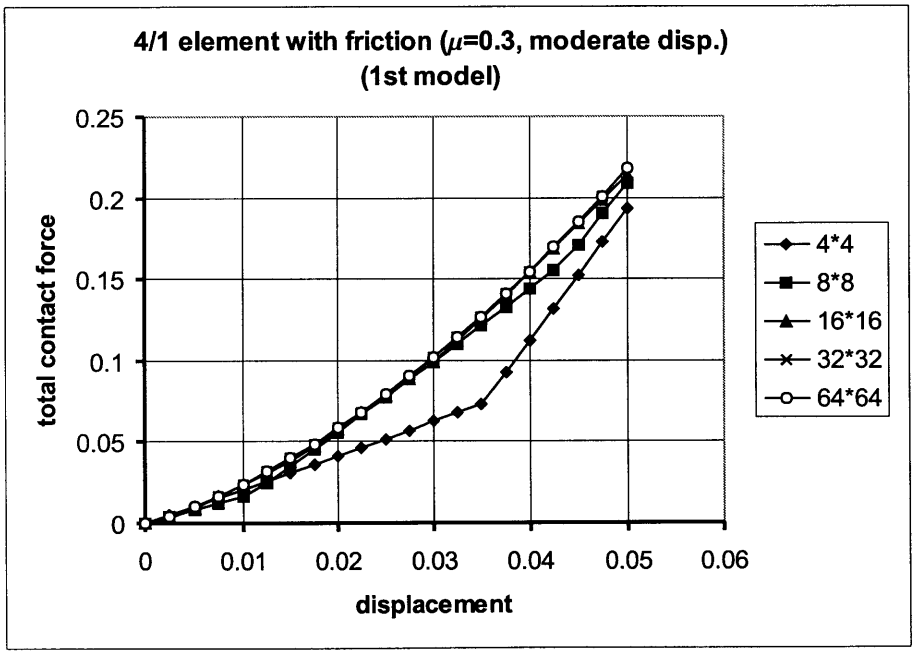

Figure 4-13: Force-displacement curve for the cylindrical rubber block (1st model), $\Delta = 0.05m$ (4/1 elements with friction)

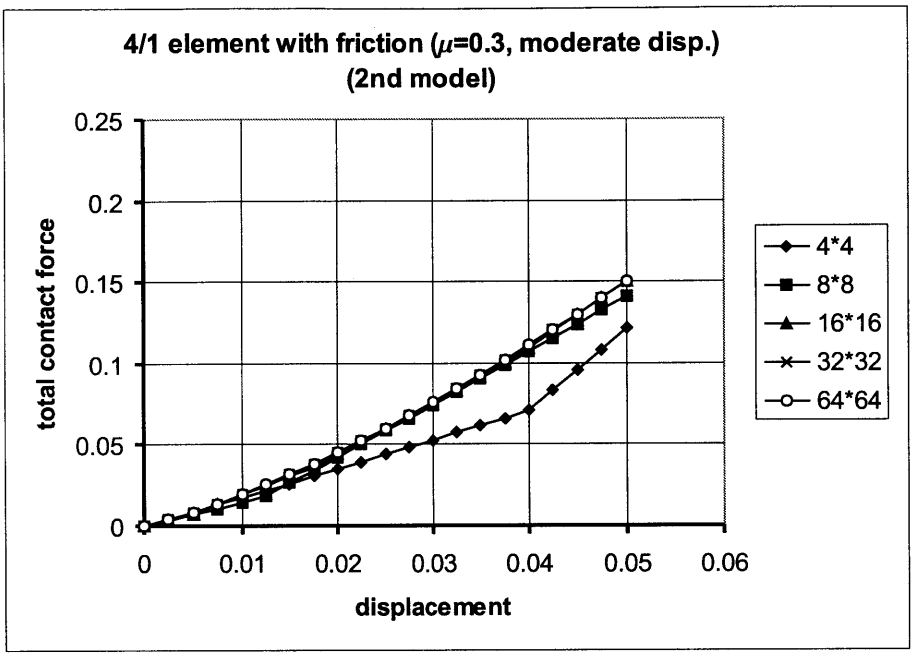

Figure 4-14: Force-displacement curve for the cylindrical rubber block (2nd model), $\Delta = 0.05m$ (4/1 elements with friction)

displacement conditions ($\Delta = 0.25m$) are considered. To simulate the load application, the vertical displacement is prescribed along the top surface of the model. In the case of moderate displacement conditions, the load (displacement, Δ) is applied in twenty equal load steps and in the case of large displacement condition the automatic-time-stepping method (ATS) is used to obtain converged solutions, which is implemented in ADINA (see Theory and Modelling Guide Volume 1: ADINA). Figures 4-13 to 4-16 show the force-displacement relationship for moderate displacements. Considering figure 4-13, we see that near $\Delta = 0.035$ for the 4×4 mesh, the stiffness of the mesh changes noticeably. In the output, we can find that below $\Delta = 0.035$, only one node is in contact and above $\Delta = 0.035$, three nodes are in contact. This means that the model is artificially soft below $\Delta = 0.035$. We can also see this phenomenon using the 8×8 mesh (near $\Delta = 0.0125$ and $\Delta = 0.045$). We can find another interesting observation in this figure, namely, that contrary to the rectangular rubber block, finer meshes are stiffer than coarser meshes. The reason

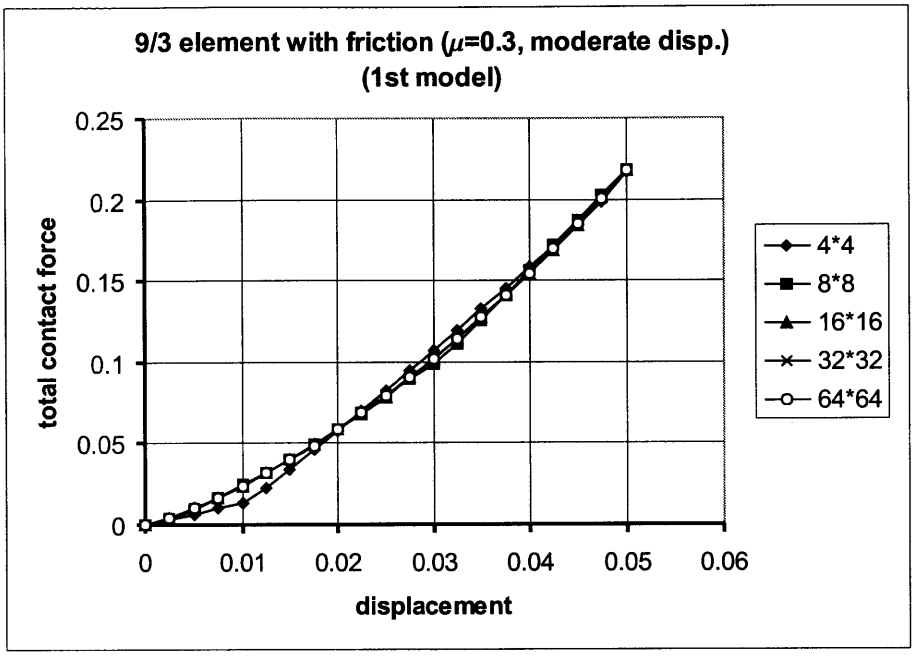

Figure 4-15: Force-displacement curve for the cylindrical rubber block (1st model), $\Delta = 0.05m$ (9/3 elements with friction)

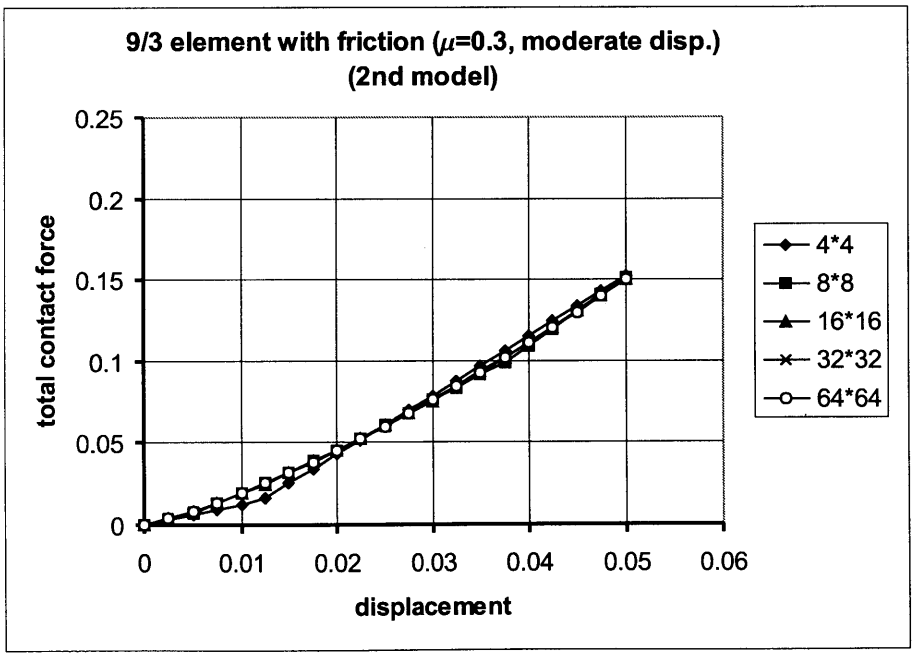

Figure 4-16: Force-displacement curve for the cylindrical rubber block (2nd model), $\Delta = 0.05m$ (9/3 elements with friction)

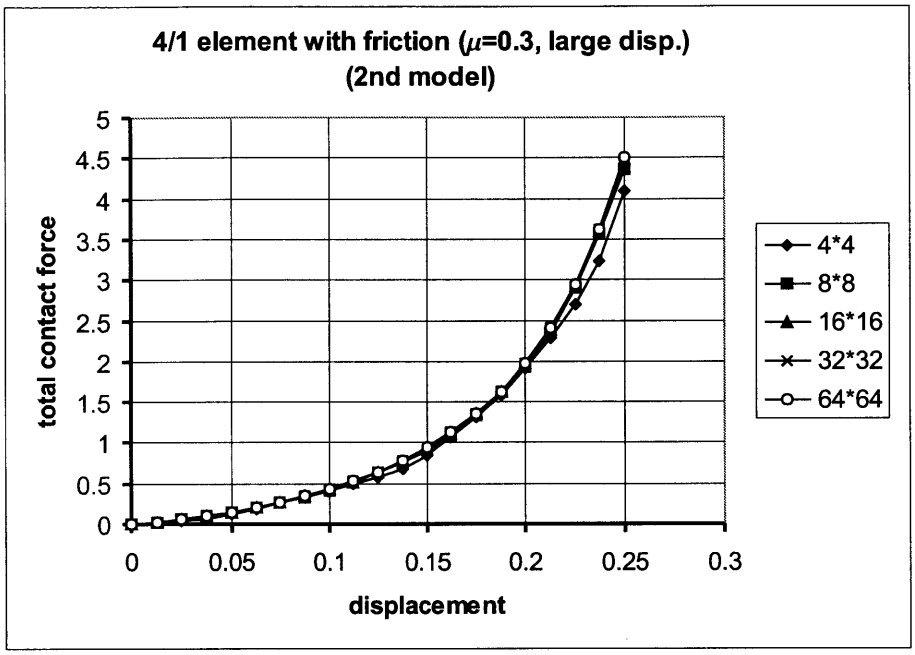

Figure 4-17: Force-displacement curve for the cylindrical rubber block (2nd model), $\Delta = 0.25m$ (4/1 elements with friction)

is that when there are more nodes in contact, the model becomes stiffer in spite of the fact that generally coarser meshes are stiffer than finer meshes. The 2nd model (see figure 4-14) represents a similar solution pattern as the 1st model except that the total contact force is smaller, in each time (load) step, than for the 1st model. Figures 4-15 and 4-16 show the results using the 9/3 elements. Here, we can see that the range of values concerning the predicted contact forces is smaller in each time step compared with the 4/1 element solutions, which means that the results of the five element meshes are in close agreement with each other.

For the large displacement solution, the resulting force-displacement curves are shown in figures 4-17 and 4-18. The five solutions using 9/3 elements are in closer agreement with each other than those using 4/1 elements, as in the above results, and both results show that as $\Delta = 0.25$ is approached, the stiffness of the cylindrical rubber block increases drastically, which agrees with the rubber material behavior in the compression part shown in figure 4-2.

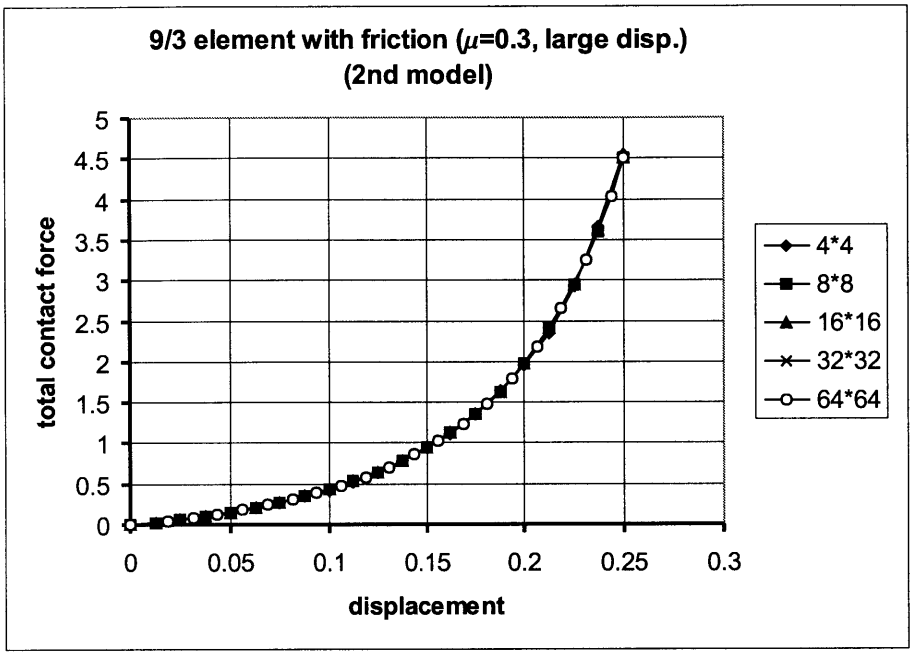

Figure 4-18: Force-displacement curve for the cylindrical rubber block (2nd model), $\Delta = 0.25m$ (9/3 elements with friction)

4.4 Example 3 - Analysis of Rubber Sheet in a Converging Channel

A sheet of rubber in plane stress conditions moves in a rigid horizontal channel, see figure 4-19 (a). The right face of the sheet is subjected to the displacement history given in figure 4-19 (b) making this a large deformation problem. The displacements are assumed to vary slowly so that inertia effects can be neglected. To model the sheet of rubber, 4/1 elements for both a 12×4 mesh and a 24×8 mesh (case 1 and 2) are used and 9/3 elements for a 12×4 mesh (case 3) are used. Figure 4-20 shows the finite element idealization of the 12×4 mesh of 4/1 elements. In all cases, the friction coefficient $\mu = 0.15$ is used and Mooney-Rivlin constants $C_1 = 25.0$ and $C_2 = 7.0$ are used. Here, we use both the segment method and the constraint function method and compare the results (in the above two examples, we used only the constraint function method).

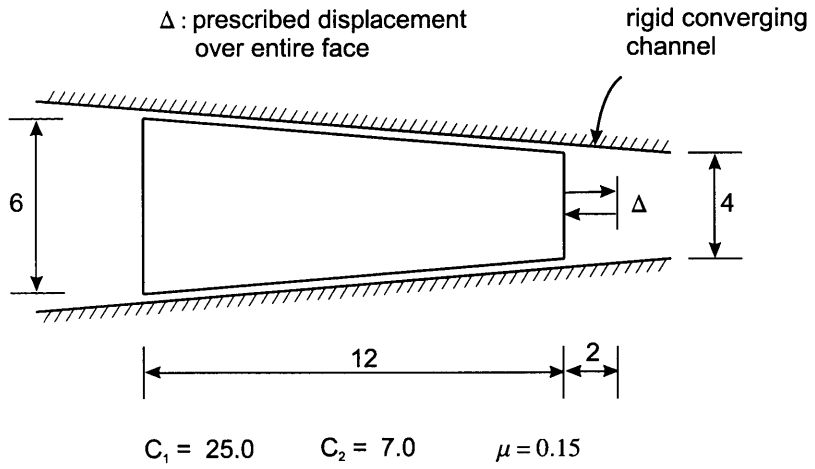

(a) Problem considered

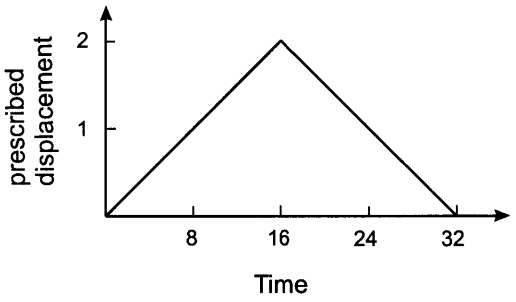

(b) Prescribed displacement

Figure 4-19: Rubber sheet in a converging channel: (a) problem considered; (b) prescribed displacement

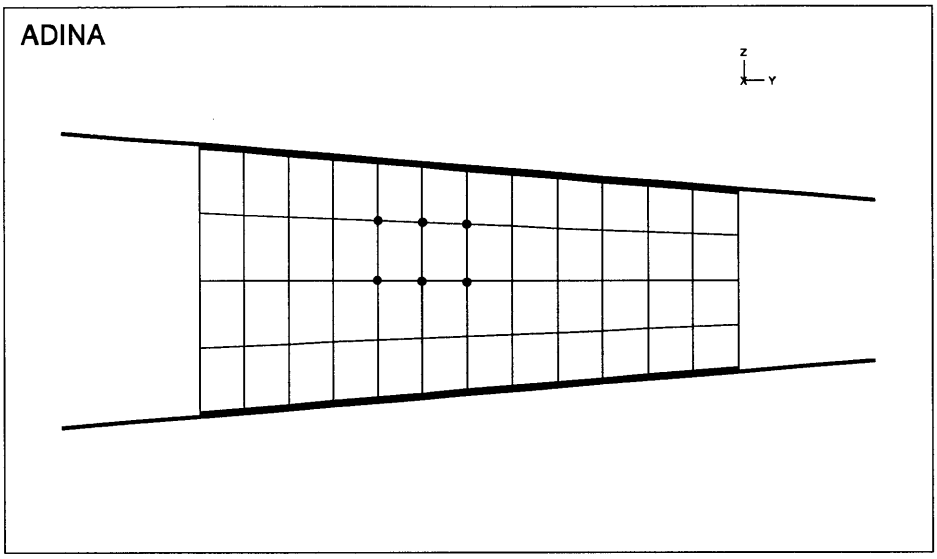

Figure 4-20: Mesh used for the rubber sheet in a converging channel (4/1 elements, 12×4 mesh)

Figures 4-21 to 4-24 show the distribution of normal and tangential tractions for different load steps in each solution. We see that the results of both methods are in close correspondence except near the face at which the displacements are imposed. However, we can also see that the constraint function method gives more reasonable results than the segment method in tangential tractions near the face. Using the 12×4 mesh (figures 4-21 and 4-22) and 24×8 mesh (figures 4-23 and 4-24) of 4/1 elements, a close agreement is observed between the results although the 12×4 mesh represents a coarse idealization of the rubber sheet. Figures 4-25 and 4-26 show the distributions of normal and tangential tractions for the 12×4 mesh using 9/3 elements. In this case, an element has two segments, and so this case has the same number of segments as in the 24×8 mesh using 4/1 elements. The solution shows similar patterns as the solution presented using the 24×8 mesh of 4/1 elements. But due to the two linear contact segments per parabolic displacements on an element edge, there is some oscillation in the contact tractions using the 9/3 elements. The three cases all show that at time 18 the tangential tractions have partially reversed, which means that some segments are still in sticking conditions.

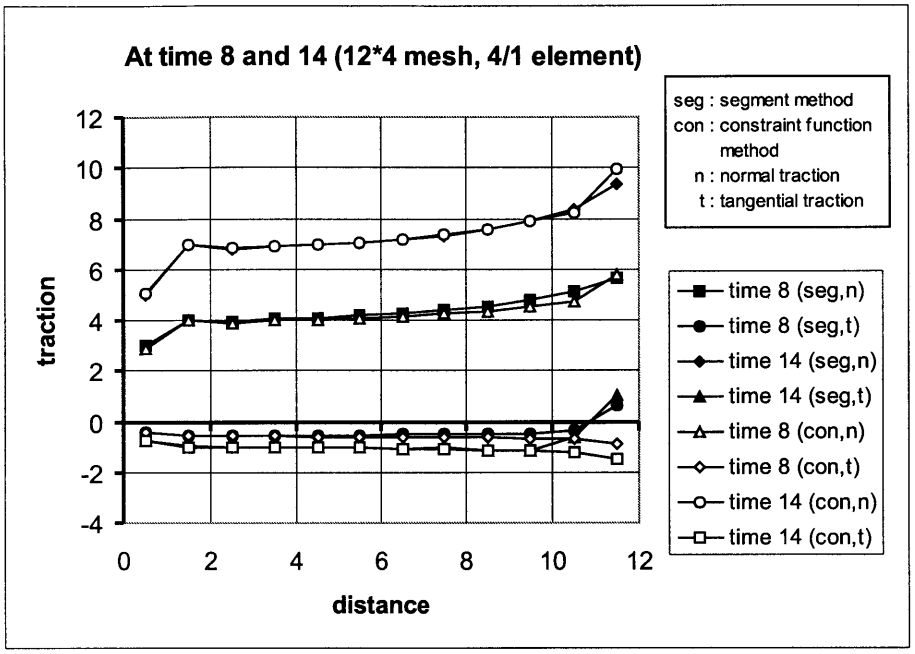

Figure 4-21: Normal and tangential tractions for the rubber sheet at times 8 and 14 (case 1 : 12×4 mesh, 4/1 elements)

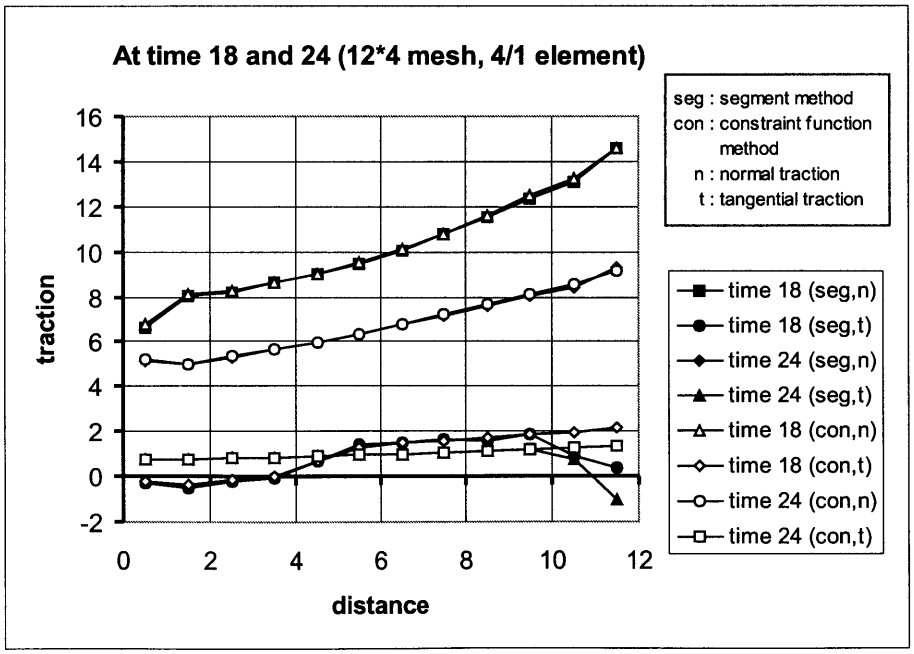

Figure 4-22: Normal and tangential tractions for the rubber sheet at times 18 and 24 (case 1 : 12×4 mesh, 4/1 elements)

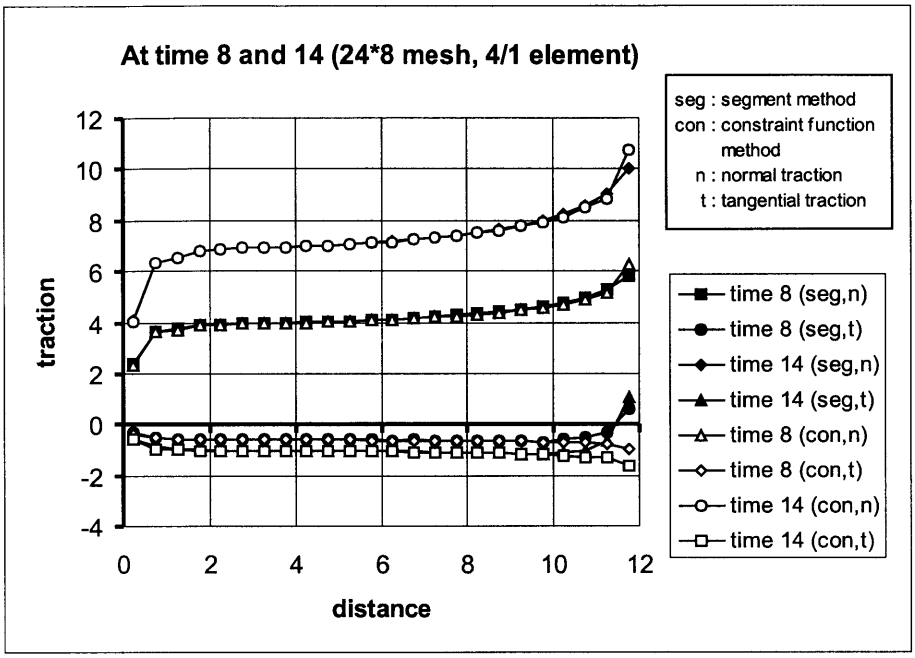

Figure 4-23: Normal and tangential tractions for the rubber sheet at times 8 and 14 (case 2 : 24×8 mesh, 4/1 elements)

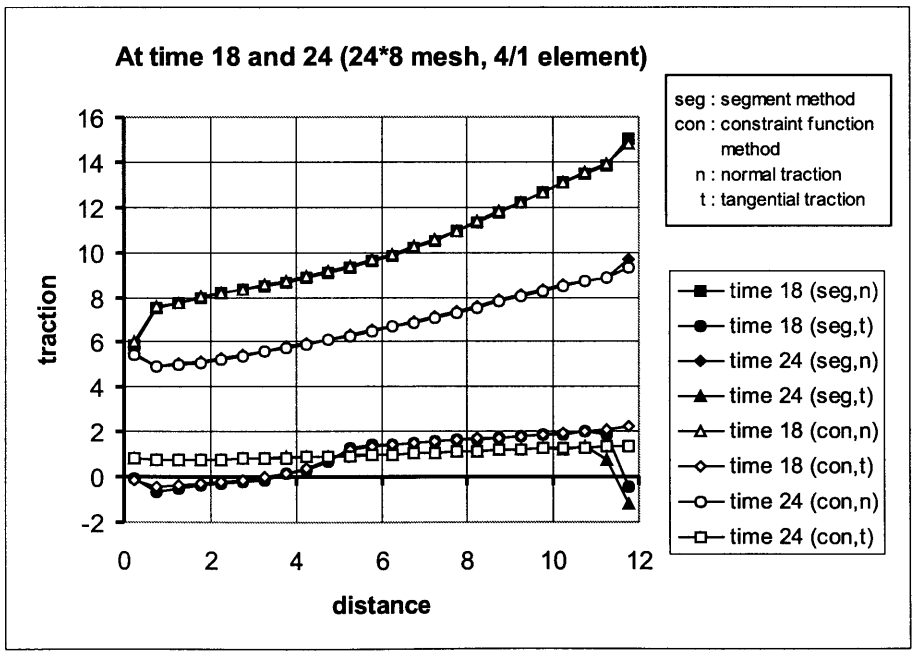

Figure 4-24: Normal and tangential tractions for the rubber sheet at times 18 and 24 (case 2 : 24×8 mesh, 4/1 elements)

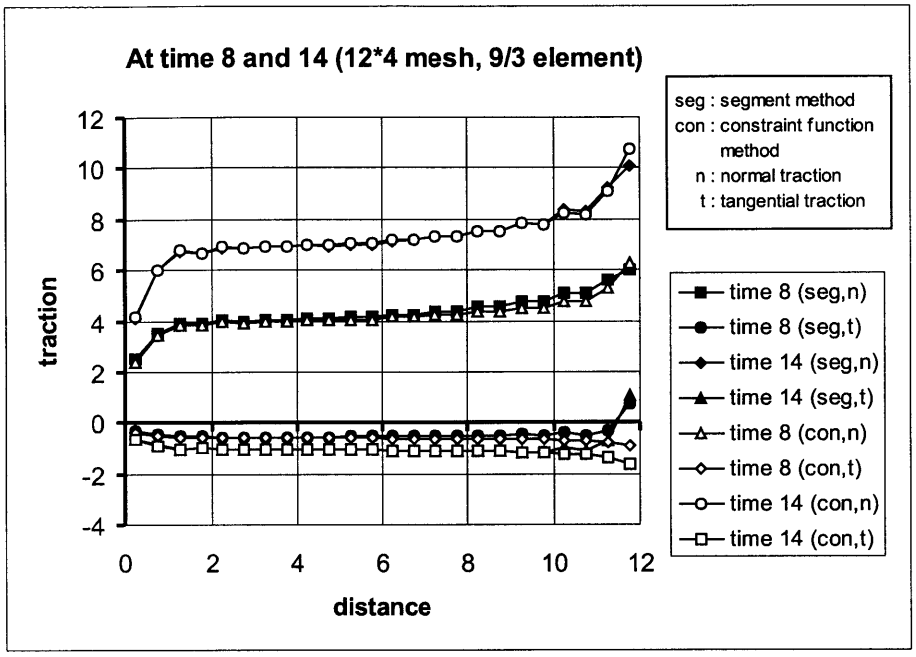

Figure 4-25: Normal and tangential tractions for the rubber sheet at times 8 and 14 (case 3 : 12×4 mesh, 9/3 elements)

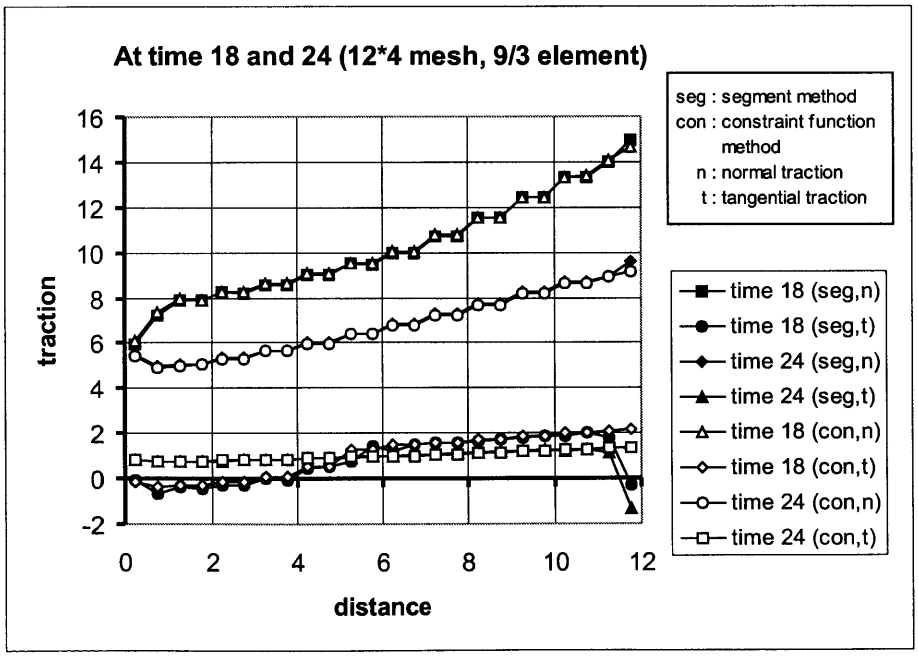

Figure 4-26: Normal and tangential tractions for the rubber sheet at times 18 and 24 (case 3 : 12×4 mesh, 9/3 elements)

Chapter 5

Concluding Remarks

For the evaluation of contact solution algorithms, we have focused on *the segment method* and *the constraint function method* which are implemented in ADINA and reviewed in detail the algorithms. We have also described the continuum formulation of contact problems where equilibrium equations and contact conditions are included for the finite element solutions, and basic solution approaches - *the Lagrange multiplier method, the penalty method and the augmented Lagrangian method.*

To evaluate the algorithms, the following three examples were considered: 1) rectangular rubber block, 2) cylindrical rubber block and 3) rubber sheet in a converging channel. In examples 1 and 2, we have evaluated the performance of finite elements using 4/1 elements and 9/3 elements with no friction and friction for moderate and large displacement conditions respectively. Example 2 is different from example 1 in that from its initial time step, the number of nodes in contact varies continuously as the load increases even for the moderate displacement condition. Here, we have found an interesting observation that finer meshes are stiffer than coarser meshes contrary to the observation for the rectangular rubber block. The reason is that when there are more nodes in contact the model becomes stiffer in spite of the fact that generally coarser meshes are stiffer than finer meshes. In example 3, we have used both the segment method and the constraint function method and compared the results. We observed that the results of both methods are in close correspondence except near

the face at which the displacements are imposed and the constraint function method predicts more reasonable results than the segment method for the tangential tractions near the face.

It should be mentioned that the solution using the constraint function method may be sensitive to the choice of time stepping, depending on the physical problem solved, although the method enforces the contact and friction inequality constraints explicitly and does not require an active set procedure. In particular, if in the solution ϵ_t (a small parameter in equation (3.45)) is of a very small value, small incremental load steps should be employed even when using the automatic-time-stepping method (ATS). Here it could be more effective to automatically adjust the value of ϵ_t to reach faster convergence.

Comparing the 4/1 and 9/3 element solutions, we have found that the 9/3 element is clearly more powerful but it would be valuable to use a quadratic contact segment rather than two linear contact segments on the element sides.

Finally, the improvements proposed by N. El-Abbasi and K.J. Bathe [4] should be further researched and should be evaluated using the three proposed test problems of this thesis.

Bibliography

[1] K. J. Bathe, *Finite Element Procedures*, Prentice Hall, 1996

[2] K. J. Bathe and A. Chaudhary, A solution method for planar and axisymmetric contact problems, *International Journal for Numerical Methods in Engineering*, Vol. 21, pp. 65-88, 1985

[3] A. L. Eterovic and K. J. Bathe, On the treatment of inequality constraints arising from contact conditions in finite element analysis, *Computers & Structures*, Vol. 40, pp. 203-209, 1991

[4] N. El-Abbasi and K. J. Bathe, Stability and patch test performance of contact discretizations and a new solution algorithm, *Computers & Structures*, Vol. 79, pp. 1473-1486, 2001

[5] K. J. Bathe and P. A. Bouzinov, On the constraint function method for contact problems, *Computers & Structures*, Vol. 64, pp. 1069-1085, 1997

[6] P. Papadopoulos and J. M. Solberg, A Lagrange multiplier method for the finite element solution of frictionless contact problems, *Mathematical and computer modelling*, Vol. 28, pp. 373-384, 1998

[7] G. Zavarise and P. Wriggers, A segment-to-segment contact strategy, *Mathematical and computer modelling*, Vol. 28, pp. 497-515, 1998

[8] W. N. Liu, T. Huemer, J. Eberhardsteiner, and H. A. Mang, Modified node-smoothing method of non-smooth surfaces in FE analyses of 2D contact, *Computers & Structures*, Vol. 80, pp. 2185-2193, 2002

[9] P. Wriggers and L. Krostulovic-Opera, On smooth finite element discretization for frictional contact problems, *GAMM '99*, Book of Abstracts, Metz, France, April 12-16, pp. 164, 1999

[10] N. Kikuchi, A smoothing technique for reduced integration penalty methods in contact problems, *International Journal for Numerical Methods in Engineering*, Vol. 18, pp. 343-350, 1982

[11] N. Kikuchi and Y. J. Song, Remarks on relations between penalty and mixed finite element methods for a class of variational inequalities, *International Journal for Numerical Methods in Engineering*, Vol. 15, pp. 1557-1561, 1980

[12] J. T. Oden, Exterior penalty methods for contact problems in elasticity, In W. Wunderlich, E. Stein, and K. J. Bathe, editors, *Nonlinear Finite Element Analysis in Structural Mechanics: Proceedings of the Europe-U.S. Workshop*, Springer-Verlag, July 1981

[13] P. Wriggers, J. C. Simo and R. L. Taylor, Penalty and augmented Lagrangian formulations for contact problems, In J. Middleton and G. H. Pande, editors, *Proceedings of the International Conference on Numerical Methods in Engineering Theory and Applications, NUMETA '85*, pp. 97-106, January 1985

[14] R. Glowinski, P. Le Tallec and M. Vidrascu, Augmented Lagrangian techniques for solving frictionless contact problems in finite elasticity, In P. G. Bergan, K. J. Bathe, and W. Wunderlich, editors, *Finite Element Methods for Nonlinear Problems: Proceedings of the Europe-U.S. Symposium*, Springer-Verlag, August 1985

[15] D. Y. Yang, D. G. Ahn, C. H. Lee, C. H. Park, T. J. Kim, Integration of CAD/CAM/CAE/RP for the development of metal forming process, *Journal of Materials Processing Technology*, Vol. 125-126, pp. 26-34, 2002